

Two active species from a single metal halide precursor: a case study of highly productive Mn-catalyzed dehydrogenation of amine-boranes via intermolecular bimetallic cooperation

Ekaterina S. Gulyaeva,^{†,‡} Elena S. Osipova,[‡] Sergey A. Kovalenko,[‡] Oleg A. Filippov,^{‡,*} Natalia V. Belkova,[‡] Laure Vendier,[†] Yves Canac,^{†,*} Elena S. Shubina^{‡,*} and Dmitry A. Valyaev^{†,*}

[†] LCC-CNRS, Université de Toulouse, CNRS, 205 route de Narbonne 31077 Toulouse, Cedex 4, France. E-mails: dmitry.valyaev@lcc-toulouse.fr, yves.canac@lcc-toulouse.fr

[‡] A. N. Nesmeyanov Institute of Organoelement Compounds (INEOS), Russian Academy of Sciences, 28/1 Vavilov str., GSP-1, B-334, Moscow, 119334, Russia

E-mails: h-bond@ineos.ac.ru, shu@ineos.ac.ru

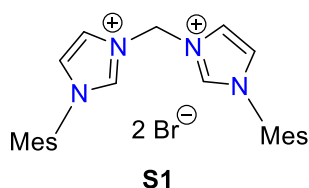
Electronic Supplementary Information

Table of contents

Experimental part and synthesis of Mn(I) complexes	S3
X-ray diffraction details.....	S5
Figure S1. Molecular structure of complex $[3^{MeCN}](BF_4)$	S5
Figures S2-S10. NMR spectra of compounds S1 , 3^{Br} , 3^H , $[3^{MeCN}](BF_4)$ and $[3^{Me_3NBH_3}](BPh_4)$	S6
Pressure vs. time studies of amine-boranes dehydrogenation	S11
Figure S11. Typical kinetic curve (Δp vs. time) for catalytic H ₂ production from DMAB.....	S11
Figure S12. Kinetic curves for DMAB dehydrogenation at 60°C with variable catalyst charge.....	S12
Figure S13. Kinetic curves (Δp vs. time) for H ₂ production from <i>t</i> BuNH ₂ BH ₃ and MeNH ₂ BH ₃	S12
Table S1. Additional optimization data for catalytic DMAB dehydrogenation.....	S13
Figures S14-S16. ¹¹ B NMR spectra of crude amine-borane dehydrogenation products.....	S14
Table S2. Experimental ¹¹ B NMR data for DMAB and its dehydrogenation products.....	S15
Table S3. Experimental ¹¹ B NMR data for <i>t</i> BuNH ₂ BH ₃ and its dehydrogenation products.....	S16
Table S4. Experimental ¹¹ B NMR data for MeNH ₂ BH ₃ and its dehydrogenation products.....	S16
IR spectroscopy monitoring details.....	S17
Figure S17. Band decomposition for IR spectrum at the end of DMAB dehydrogenation.....	S17
Figure S18. IR monitoring for DMAB dehydrogenation in CH ₂ Cl ₂ (ν_{BH} range).....	S17
Figure S19. IR monitoring for DMAB dehydrogenation in PhCl (ν_{CO} and ν_{BH} range).....	S18
Table S5. Experimental ν_{CO} frequencies for Mn(I) complexes in PhCl and CH ₂ Cl ₂	S18
NMR spectroscopy monitoring details and characterization data for $[3^{DMAB}](BPh_4)$	S19
Figures S20-S25. ¹ H, ¹¹ B, and ¹³ C NMR monitoring for catalytic DMAB dehydrogenation.....	S20
Determination of kinetic parameters and estimation of KIE.....	S24
Figure S26. Eyring plot for the determination of ΔH for DMAB dehydrogenation in PhCl.....	S24
Table S6. Experimental initial rates of DMAB dehydrogenation in PhCl in 30–60°C range.....	S24
Figure S27. Plot of v_0 vs. c_0 for different concentrations of DMAB in PhCl at 50°C.....	S25
Figure S28. Plot of v_0 vs. $\alpha(3^{Br})$ for DMAB dehydrogenation at 50°C in PhCl.....	S25
Table S7. Experimental initial rates for KIE estimation of DMAB dehydrogenation at 60°C.....	S25
Figure S29. Plot of v_0 vs. c_0 for different concentrations of NaBPh ₄ in PhCl at 60°C.....	S26
Table S8. Experimental DMAB dehydrogenation rates upon variation of NaBPh ₄ amount.....	S26
Analysis of kinetic data and mechanistic model.....	S27
DFT calculations.	S28
Figure S30. Optimized geometry of different isomers of hydride complex 3^H	S28
Table S9. Calculated thermodynamic parameters for two isomers of Mn(I) complexes.....	S28
Figure S31. Optimized geometry of 3^H...DMAB and PES scan on its attempted deprotonation.....	S29
Figure S32. Optimized geometry of facial isomers of cationic complex 3⁺	S29
Figure S33. Optimized geometry of 3^{DMAB+} and PES scan on its attempted hydride ⁺ transfer.....	S29
Figure S34. ΔG^{298} and ΔH^{298} profiles for DMAB dehydrogenation catalyzed by 3⁺/3^H couple.....	S30
Figure S35. Optimized geometry of binuclear complexes 4⁺ and 5...3^{H2+}	S30
Figure S36. Optimized geometry of mononuclear complexes 3^{H2+} , 5 and 3^H...BH₂=NMe₂	S31
References.....	S32

Experimental part.

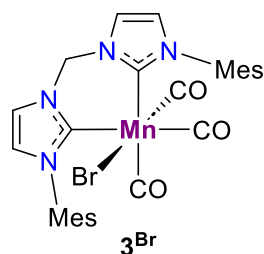
General considerations. All manipulations were performed using standard Schlenk techniques under an atmosphere of dry nitrogen or argon. Dry and oxygen-free organic solvents (THF, toluene, CH₂Cl₂, Et₂O, MeCN, pentane) were obtained using LabSolv (Innovative Technology) solvent purification system. Commercially available HPLC grade DMF was degassed by argon bubbling during 15 min through and stored over 4 Å molecular sieves. Reagent grade hexane used for crystallization was degassed by nitrogen bubbling for 15 min prior to use. Other solvents PhCl, PhF and *n*BuCl were stored over CaH₂ and distilled under inert atmosphere prior to use. Deuterated solvents for NMR spectroscopy were degassed before use by three freeze-pump-thaw cycles and kept over 4 Å molecular sieves. Commercially available amine-boranes (Me₂NHBH₃, *t*BuNH₂BH₃, MeNH₂BH₃, NH₃BH₃, Me₃NBH₃) and [Ph₃C](B(C₆F₅)₄) were purified by sublimation under static vacuum and recrystallization from CH₂Cl₂/Et₂O mixture, respectively. Deuterated amine-borane derivatives (Me₂NDBH₃, Me₂NHBD₃, Me₂NDBD₃),¹ *N*-mesitylimidazole,² Mn(I) complexes **1**^H,³ [**1**^{*n*BuCl}](B(C₆F₅)₄)³ and [**2**^{*n*BuCl}](B(C₆F₅)₄)⁴ were prepared as previously described. Cationic complex [**3**^{*n*BuCl}](B(C₆F₅)₄) was generated by the treatment of Mn(I) hydride **3**^H with [Ph₃C](B(C₆F₅)₄) in *n*BuCl at -90°C. Bis-imidazolium salt **S1**² and hydride complexes **2**^H⁵ and **3**^H⁶ were synthesized by slightly modified literature procedures. Reagent grade chemicals Mn(CO)₅Br, CH₂Br₂, AgBF₄, NaBPh₄ were utilized without additional purification. ¹H, ¹¹B, and ¹³C NMR spectra were recorded on Bruker Avance 400, Avance III HD 400, Avance 600 Neo spectrometers and calibrated against the residual signals of the deuterated solvents (¹H and ¹³C) and BF₃·OEt₂, (¹¹B internal standard). IR spectra were measured in 0.01-0.1 cm CaF₂ cells on Nicolet iS50 and PerkinElmer Frontier FT-IR spectrometers and are given in cm⁻¹ with relative intensity in parenthesis. Elemental analyses were carried out at the LCC-CNRS (Toulouse) using Perkin Elmer 2400 series II analyzer.



Modified synthesis of bis-imidazolium salt S1. *N*-mesitylimidazole (2.18 g, 11.7 mmol), CH₂Br₂ (0.40 mL, 5.85 mmol) and dry DMF (5 mL) were charged in nitrogen filled Schlenk tube. The reaction mixture was placed in an oil-bath preheated to 100°C and stirred at this temperature under inert atmosphere for 2 days. Then DMF was removed under reduced pressure and the residue was washed with Et₂O (2×20 mL). The

resulting product was dissolved in CH₂Cl₂ (30 mL) and Et₂O (40-50 mL) was added dropwise under vigorous stirring to induce precipitation of white solid. The resulting suspension was stirred for 15 min and the supernatant was removed using a cannula tipped with filter paper. The precipitate was washed with Et₂O (2×20 mL) and dried in vacuum affording bis-imidazolium salt **S1** (2.72 g, 85% yield) as a white powder. Analytical data were consistent with literature data.²

S1: ¹H NMR (400.1 MHz, CDCl₃, 25°C): δ 11.40 (s, 2H, CH_{Im-2}), 9.88 (s, 2H, NCH₂N), 7.97 (s, 2H, CH_{Im-4,5}), 7.20 (s, 2H, CH_{Im-4,5}), 7.04 (s, 4H, CH_{Mes}), 2.36 (s, 6H, CH_{3 para-Mes}), 2.05 (s, 12H, CH_{3 ortho-Mes}).



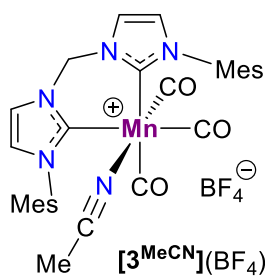
Optimized synthesis of complex 3^{Br}. Solid K₂CO₃ (2.2 g, 15.9 mmol) in a Schlenk tube was dried under vacuum at ~80°C during ca. 20 min. The reaction vessel was then cooled to room temperature and charged with Mn(CO)₅Br (363 mg, 1.32 mmol), imidazolium salt **S1** (722 mg, 1.32 mmol) and 15 mL of dry DMF. The resulting suspension was sonicated for 3 min, placed in an oil-bath preheated to 120°C and vigorously stirred at this temperature for 3-4 hours. The reaction progress was controlled by IR monitoring by taking an aliquot of reaction mixture, removal of DMF under

vacuum and dissolution of the residue in THF. When only ν_{CO} bands of the target product **3^{Br}** (2009, 1928, 1887 cm⁻¹) were observed in IR spectrum, the reaction mixture was cooled to ~50°C and DMF was removed under reduced pressure at this temperature. In order to remove entirely traces of DMF from the residue toluene (15 mL) was added, the resulting suspension was sonicated for 10 min and evaporated under vacuum. The product was repeatedly extracted with CH₂Cl₂ (5×10 mL) under sonication until the complete disappearance of yellow color of remained solid. The extracts were filtered through Celite pad, concentrated to a half of initial volume and then hexane (50 mL) was

slowly added upon vigorous stirring. The resulting yellow suspension was again concentrated under reduced pressure to remove a majority of CH_2Cl_2 and left at -20°C overnight. Supernatant was removed by filtration using a cannula tipped with filter paper and the precipitate was washed with hexane (2x20 mL) and dried under vacuum affording target product 3^{Br} (663 mg, 83% yield) as yellow microcrystalline powder. Analytical data were consistent with literature data.²

3^{Br} : ^1H NMR (400.1 MHz, CDCl_3 , 25°C): δ 7.42 (d, $^2J_{\text{HH}} = 12.0$ Hz, 1H, NCH_2N), 7.34 (s, 2H, $\text{CH}_{\text{Im-4,5}}$), 7.00 (s, 2H, $\text{CH}_{\text{Im-4,5}}$), 6.93 (s, 4H, CH_{Mes}), 5.76 (d, $^2J_{\text{HH}} = 12.0$ Hz, 1H, NCH_2N), 2.33 (s, 6H, CH_3 Mes), 2.20 (s, 6H, CH_3 Mes), 1.91 (s, 6H, CH_3 Mes).

IR (THF): ν_{CO} 2009 (s), 1928 (s), 1887 (s) cm^{-1} ; IR (CH_2Cl_2): ν_{CO} 2012 (s), 1928 (s), 1892 (s) cm^{-1} ; IR (PhCl): ν_{CO} 2010 (s), 1932 (s), 1895 (s) cm^{-1} .

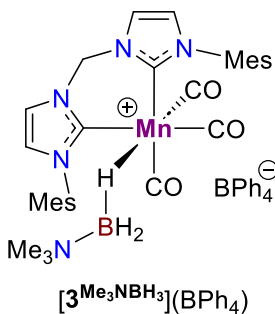


Synthesis of complex $[\mathbf{3}^{\text{MeCN}}](\text{BF}_4)$. To a mixture of solid complex 3^{Br} (241 mg, 0.4 mmol) and AgBF_4 (78 mg, 0.4 mmol) in a Schlenk tube CH_3CN (5 mL) was added upon stirring at room temperature. The resulting suspension was sonicated for 5 min and stirred until a complete consumption of starting material according to IR monitoring (15-20 min). The solution was filtered through Celite, concentrated to 1/10 of initial volume and then dry Et_2O (80 mL) was added dropwise to induce precipitation of the product finished at -20°C overnight. The supernatant was removed by decantation and the precipitate was washed with ether (2x5 mL) and dried under vacuum to afford $[\mathbf{3}^{\text{MeCN}}](\text{BF}_4)$ (211 mg, 85% yield) as pale-yellow powder. Single crystals suitable for X-ray diffraction experiments were obtained by vapor diffusion of ether into concentrated solution of $[\mathbf{3}^{\text{MeCN}}](\text{BF}_4)$ in MeCN at room temperature.

$[\mathbf{3}^{\text{MeCN}}](\text{BF}_4)$: ^1H NMR (400.1 MHz, CD_2Cl_2 , 25°C): δ 7.79 (s, 2H, $\text{CH}_{\text{Im-4,5}}$), 7.00 (s, 4H, CH_{Mes}), 6.98 (s, 2H, $\text{CH}_{\text{Im-4,5}}$), 6.52 (d, $^2J_{\text{HH}} = 13.8$ Hz, 1H, NCH_2N), 6.29 (d, $^2J_{\text{HH}} = 13.8$ Hz, 1H, NCH_2N), 2.33 (s, 6H, CH_3 Mes), 2.21 (s, 3H, CH_3 MeCN), 2.08 (s, 6H, CH_3 MeCN), 1.89 (s, 6H, CH_3 Mes).

$^{13}\text{C}\{^1\text{H}\}$ NMR (100.6 MHz, CD_2Cl_2 , 25°C): δ 219.5, 215.6 (br. s, $\text{Mn}-\text{CO}$), 190.2 (s, $\text{Mn}-\text{CN}_2$), 140.3, 136.7, 136.2 (s, $\text{C}-\text{Me}_{\text{Mes}}$), 135.8 (s, $\text{C}_{\text{ipso Mes}}$), 129.6, 129.4 (s, CH_{Mes}), 128.2 (s, $\text{Mn}-\text{NCMe}$), 124.3 (s, $\text{CH}_{\text{Im-4,5}}$), 62.8 (s, NCH_2N), 21.2, 18.3, 18.1 (s, CH_3 Mes), 4.3 (s, CH_3 MeCN).

IR (CH_2Cl_2): 2028 (s), 1940 (s), 1931 (s) cm^{-1} . Anal. Found: C, 55.46; H, 4.85; N, 10.41; Calcd. for $\text{C}_{30}\text{H}_{31}\text{BF}_4\text{MnN}_5\text{O}_3$ (M = 651.35): C, 55.32; H, 4.80; N, 10.75.



Synthesis of complex $[\mathbf{3}^{\text{Me}_3\text{NBH}_3}](\text{BPh}_4)$. To a mixture of solid 3^{Br} (50 mg, 0.08 mmol), NaBPh_4 (34 mg, 0.1 mmol) and Me_3NBH_3 (9 mg, 0.12 mmol) CH_2Cl_2 (5 mL) was added. The resulting suspension was sonicated for 5 min and stirred overnight at room temperature to give $[\mathbf{3}^{\text{Me}_3\text{NBH}_3}](\text{BPh}_4)$ as a sole product according to IR spectroscopy. The solution was filtered through Celite and evaporated under vacuum. The residue was washed with ether (2x3 mL) and dried under vacuum to afford the target product (42 mg, 54% yield) as yellow crystalline powder. Single crystals suitable for X-ray diffraction experiments were obtained by vapor diffusion of pentane into a solution of $[\mathbf{3}^{\text{Me}_3\text{NBH}_3}](\text{BPh}_4)$ in CH_2Cl_2 at room temperature.

$[\mathbf{3}^{\text{Me}_3\text{NBH}_3}](\text{BPh}_4)$: ^1H NMR (400.1 MHz, CD_2Cl_2 , 25°C): δ 7.44–7.41 (m, 8H, CH_{Ph}), 7.11–7.00 (m, 10H, CH_{Ph}), 6.99–6.86 (m, 10H, $\text{CH}_{\text{Ph}} + \text{CH}_{\text{Im-4,5}} + \text{CH}_{\text{Mes}}$), 5.74 (d, $^2J_{\text{HH}} = 13.1$ Hz, 1H, NCH_2N), 5.09 (d, $^2J_{\text{HH}} = 13.1$ Hz, 1H, NCH_2N), 2.45 (s, 9H, $\text{N}(\text{CH}_3)_3$), 2.35 (s, 6H, CH_3 Mes), 2.12 (s, 6H, CH_3 Mes), 1.83 (s, 6H, CH_3 Mes), -3.18 (br s, 3H, BH_3).

^{11}B NMR (128.4 MHz, CD_2Cl_2 , 25°C): δ -6.5 (s, BPh_4), -11.7 (br. s, BH_3).

$^{13}\text{C}\{^1\text{H}\}$ NMR (100.6 MHz, CD_2Cl_2 , 25°C): δ 222.2 (s, $\text{Mn}-\text{CO}$), 217.5 (br s, $\text{Mn}-\text{CO}$), 190.4 (s, $\text{Mn}-\text{CN}_2$), 164.3 (q, $^1J_{\text{BC}} = 49.7$ Hz, $\text{C}_{\text{ipso Ph}}$), 140.4, 136.5 (s, $\text{C}-\text{Me}_{\text{Mes}}$), 136.4 (s, CH_{Ph}), 136.2 (s, $\text{C}-\text{Me}_{\text{Mes}}$), 135.6 (s, $\text{C}_{\text{ipso Mes}}$), 129.5, 129.4 (s, CH_{Mes}), 126.3 (q, $^2J_{\text{BC}} = 3.0$ Hz, CH_{Ph}), 124.7, 123.8 (s, $\text{CH}_{\text{Im-4,5}}$), 122.5 (s, CH_{Ph}), 62.4 (s, NCH_2N), 53.8 (s, $\text{N}(\text{CH}_3)_3$), 21.3, 18.4, 18.2 (s, CH_3 Mes).

IR (CH_2Cl_2): ν_{CO} 2024 (s), 1939 (s), 1926 (s) cm^{-1} . Anal. Found: C, 67.94; H, 6.34; N, 6.99; Calcd. for $\text{C}_{55}\text{H}_{60}\text{B}_2\text{MnN}_5\text{O}_3 \times 0.8\text{CH}_2\text{Cl}_2$ (M = 983.6): C, 68.14; H, 6.31; N, 7.12.

X-ray diffraction details.

X-ray diffraction data were collected on a Xcalibur Gemini Ultra ($[3^{\text{MeCN}}](\text{BF}_4)$) and Bruker D8/APEX II/Incoatec Mo μS Microsource ($[3^{\text{Me}_3\text{NBH}_3}](\text{BPh}_4)$) diffractometers using $\text{CuK}\alpha$ ($\lambda = 1.54184 \text{ \AA}$, graphite monochromator) and $\text{MoK}\alpha$ ($\lambda = 0.71073 \text{ \AA}$, graphite monochromator) radiation, respectively. Molecular structure of complex $[3^{\text{MeCN}}](\text{BF}_4)$ is shown in Figure S1. All calculations were performed on a PC compatible computer using the WinGX system.⁸ The structures were solved using the SIR2018 program,⁹ which revealed in each instance the position of most of the non-hydrogen atoms. All the remaining non-hydrogen atoms were located by the usual combination of full matrix least-squares refinement and difference electron density syntheses using the SHELX program.¹⁰ Atomic scattering factors were taken from the usual tabulations. Anomalous dispersion terms for the Mn atoms were included in Fc. All non-hydrogen atoms were allowed to vibrate anisotropically. The most of hydrogen atoms were set in idealized positions (R_3CH , $\text{C-H} = 0.96 \text{ \AA}$; R_2CH_2 , $\text{C-H} = 0.97 \text{ \AA}$; RCH_3 , $\text{C-H} = 0.98 \text{ \AA}$; $\text{C}(\text{sp}^2)\text{-H} = 0.93 \text{ \AA}$; U_{iso} 1.2 or 1.5 times greater than the U_{eq} of the carbon atom to which the hydrogen atom is attached) and their positions refined as “riding” atoms. Three hydrogen atoms of the BH_3 moiety in $[3^{\text{Me}_3\text{NBH}_3}](\text{BPh}_4)$ were located from Fourier differences map and were refined isotropically. CCDC 2262301-2262302 contain the supplementary crystallographic data for the structures unveiled in this paper. These data can be obtained free of charge from the Cambridge Crystallographic Data Centre via www.ccdc.cam.ac.uk/data_request/cif.

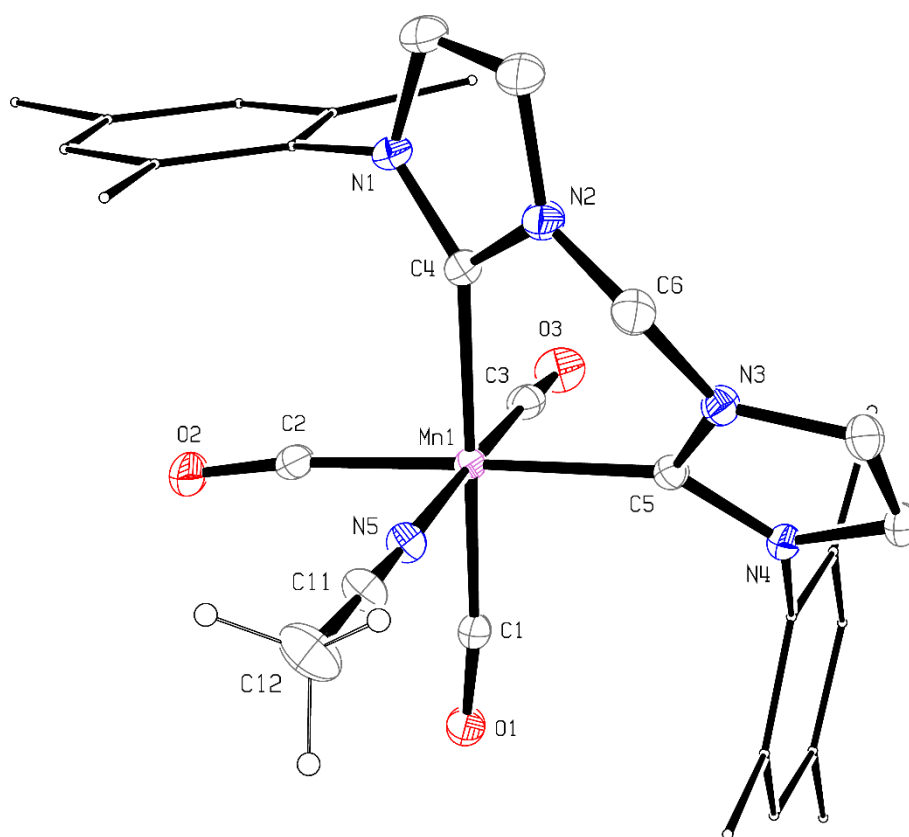


Figure S1. Molecular geometry of complex $[3^{\text{MeCN}}](\text{BF}_4)$ (20% probability ellipsoids, mesityl groups represented as wireframe, most hydrogen atoms and BF_4^- anion are not shown for clarity).

Copies of NMR spectra

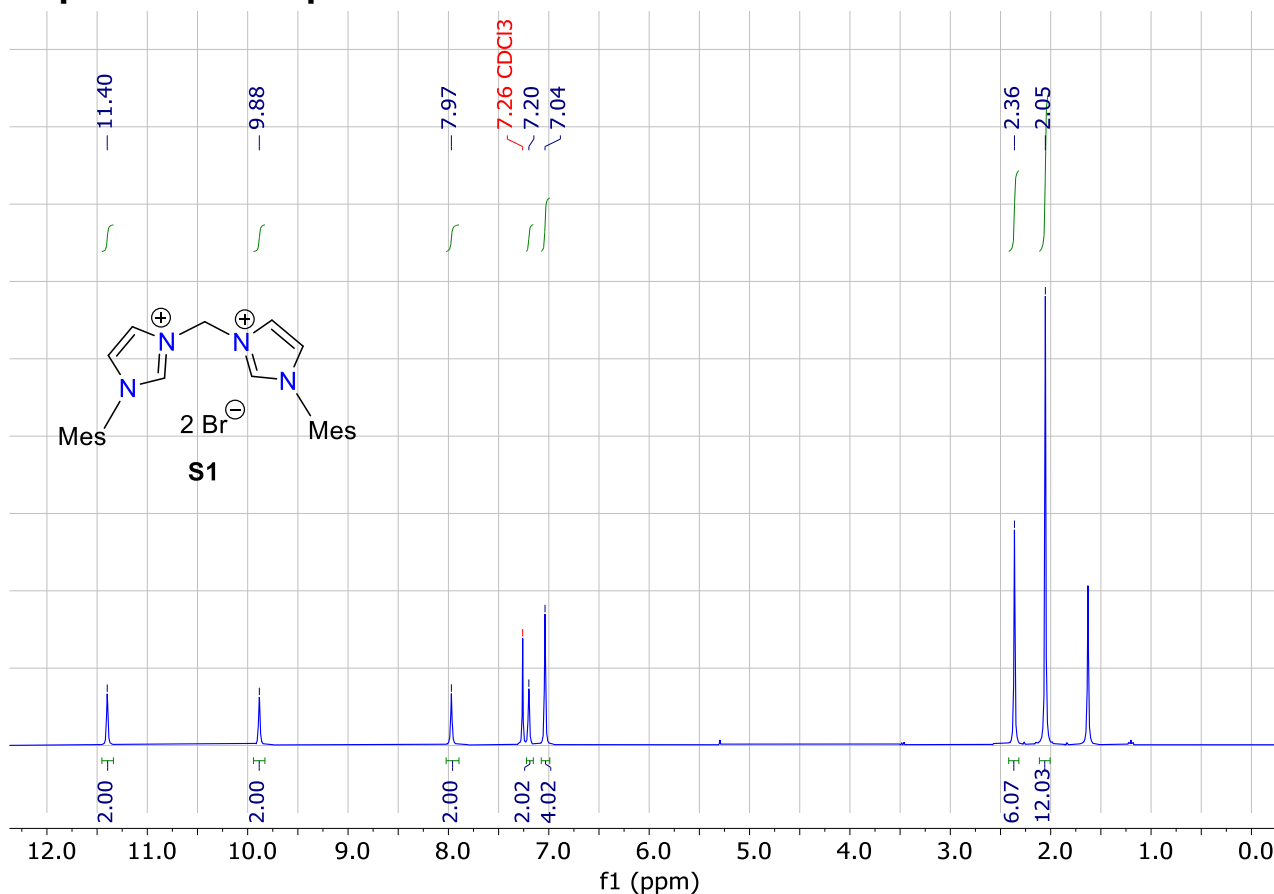


Figure S2. ^1H NMR spectrum of imidazolium salt **S1** (400.1 MHz, CDCl_3 , 25°C).

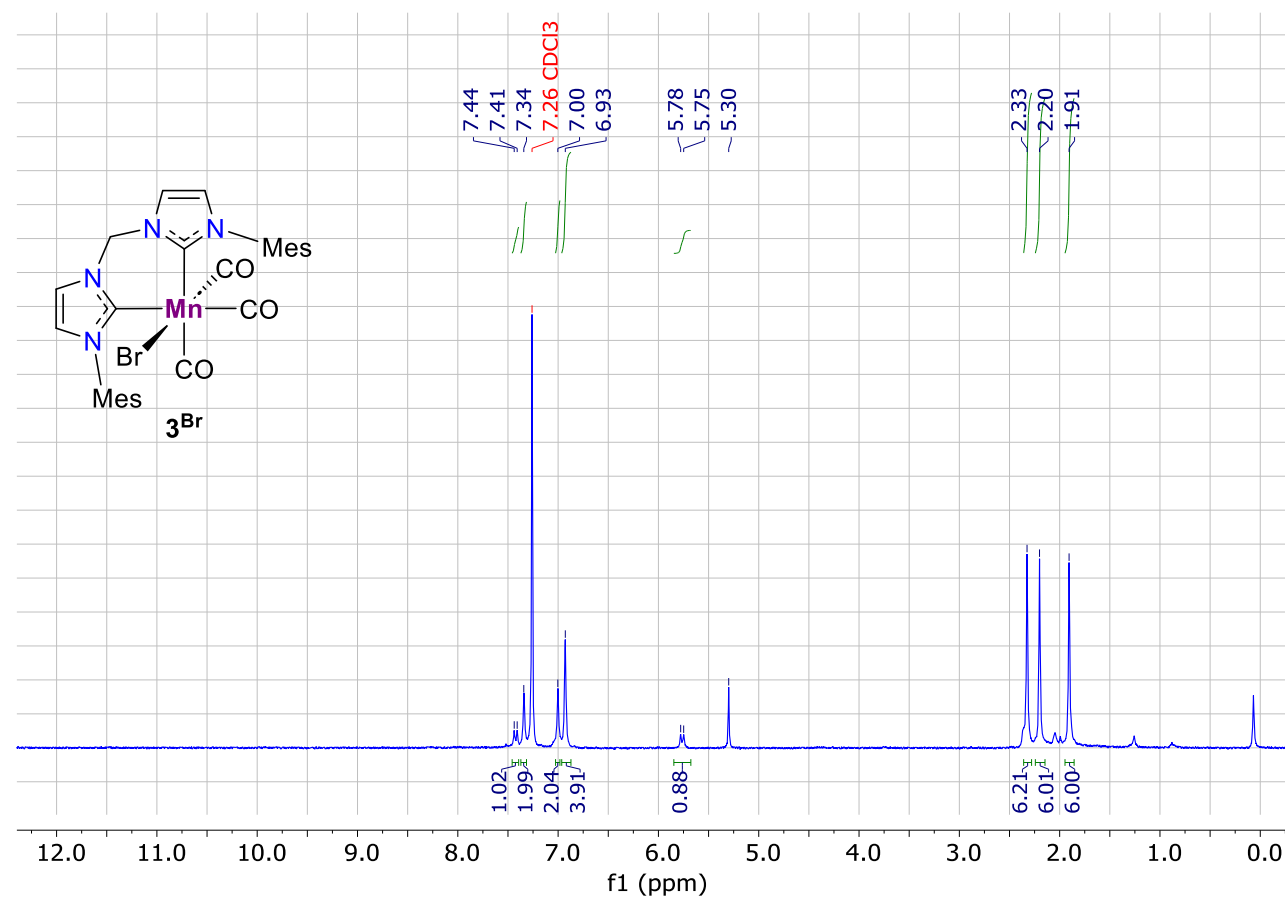


Figure S3. ^1H NMR spectrum of complex **3Br** (400.1 MHz, CDCl_3 , 25°C).

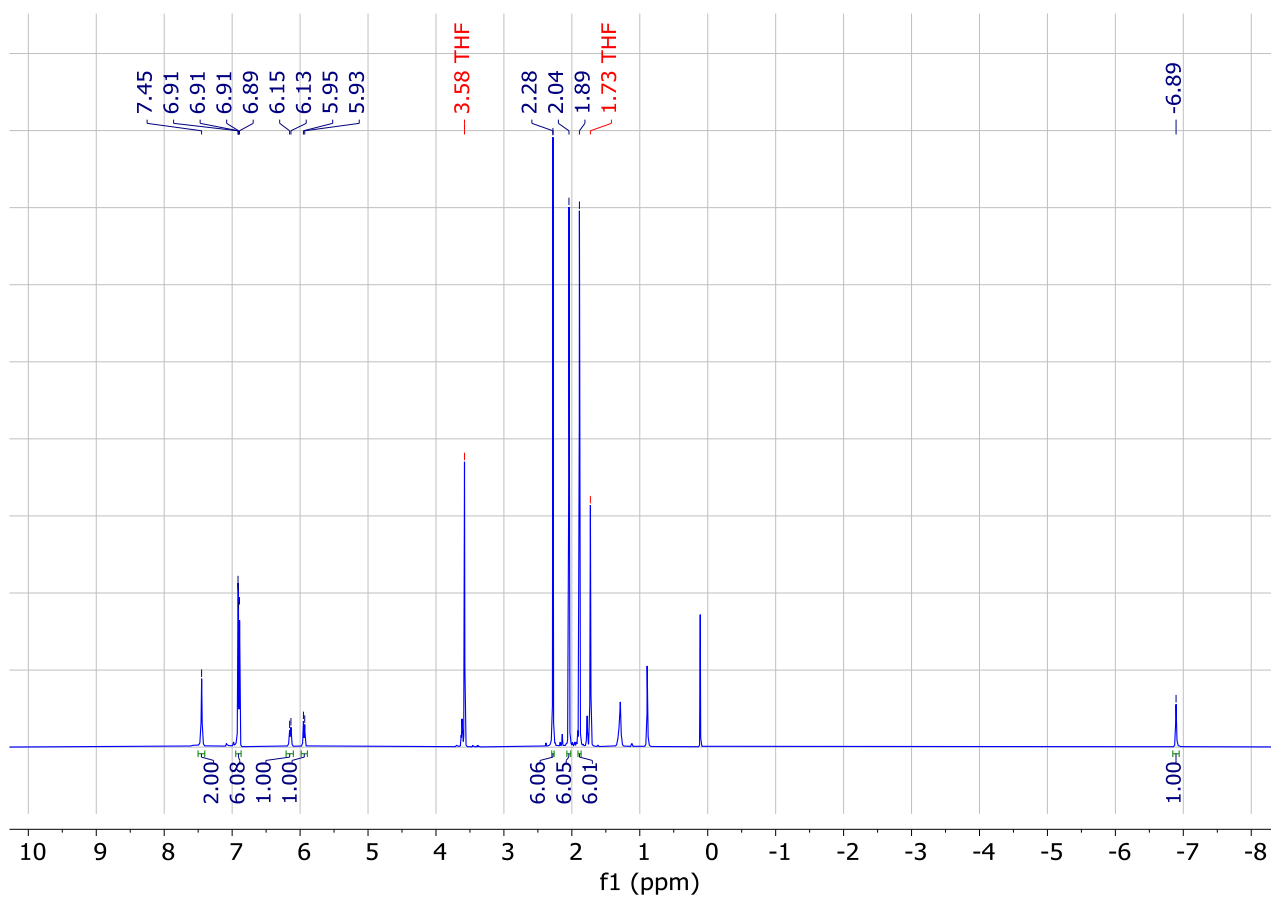


Figure S4. ^1H NMR spectrum of complex 3^{H} (600.2 MHz, $\text{THF-}d_8$, 25°C).

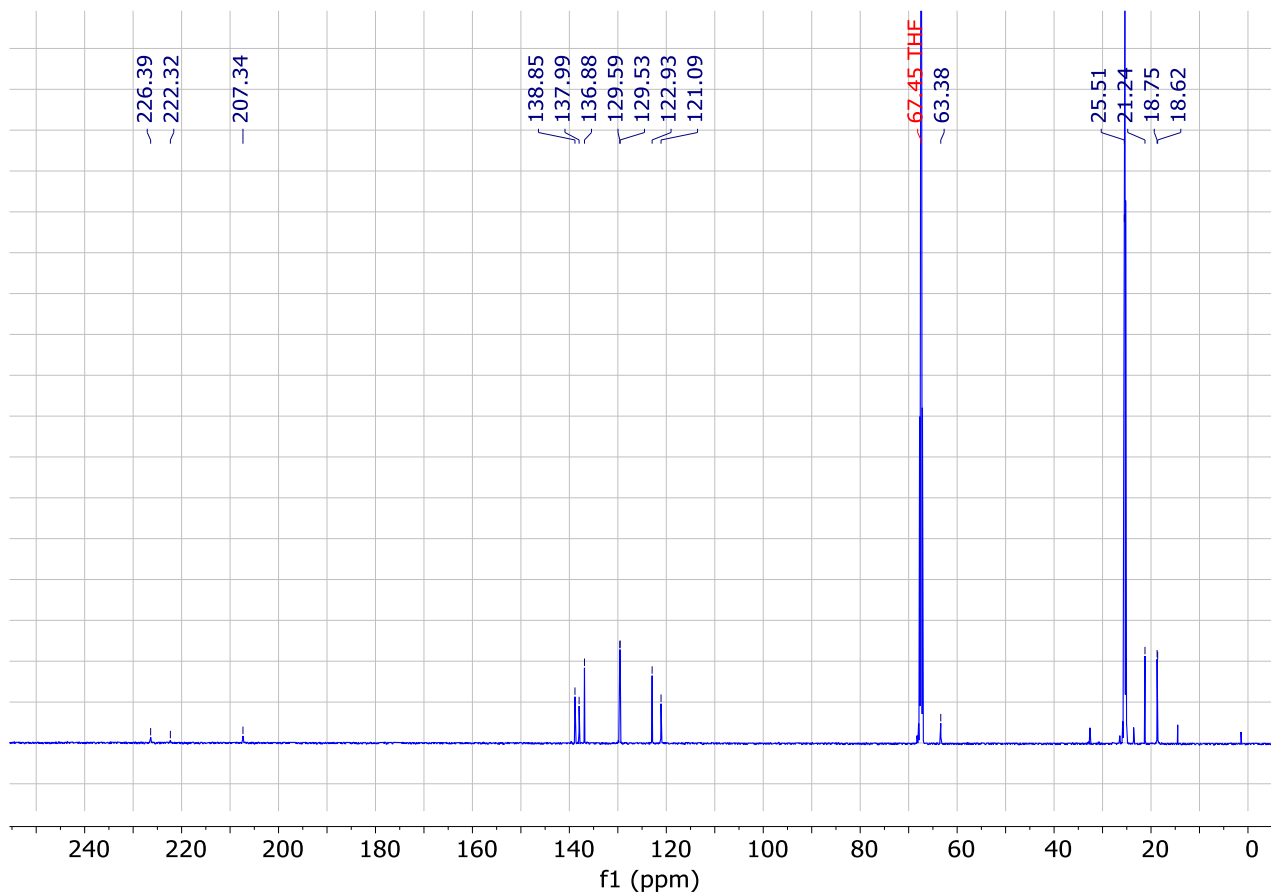


Figure S5. $^{13}\text{C}\{^1\text{H}\}$ NMR spectrum of complex 3^{H} (150.9 MHz, $\text{THF-}d_8$, 25°C).

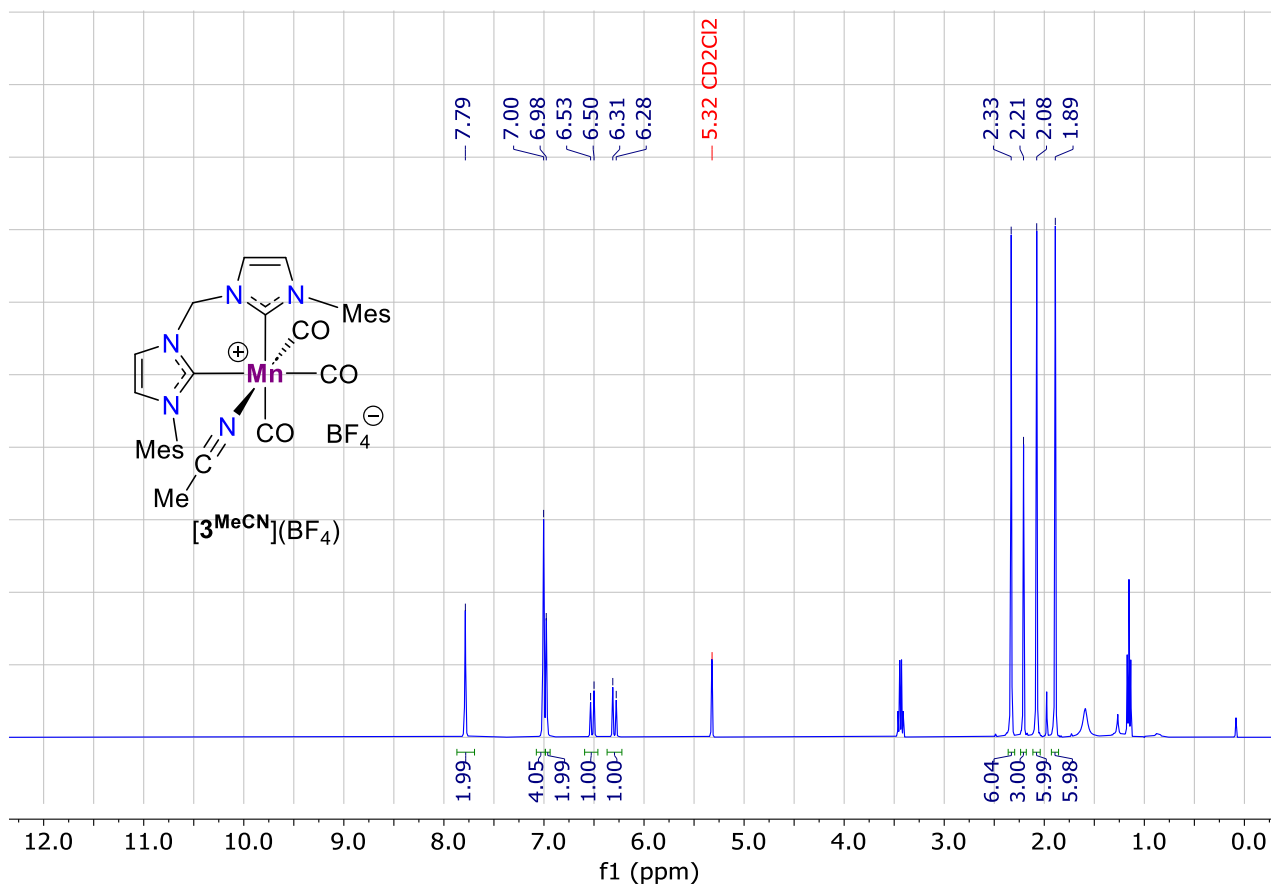


Figure S6. 1H NMR spectrum of complex $[3^{MeCN}](BF_4)$ (400.1 MHz, CD_2Cl_2 , 25°C).

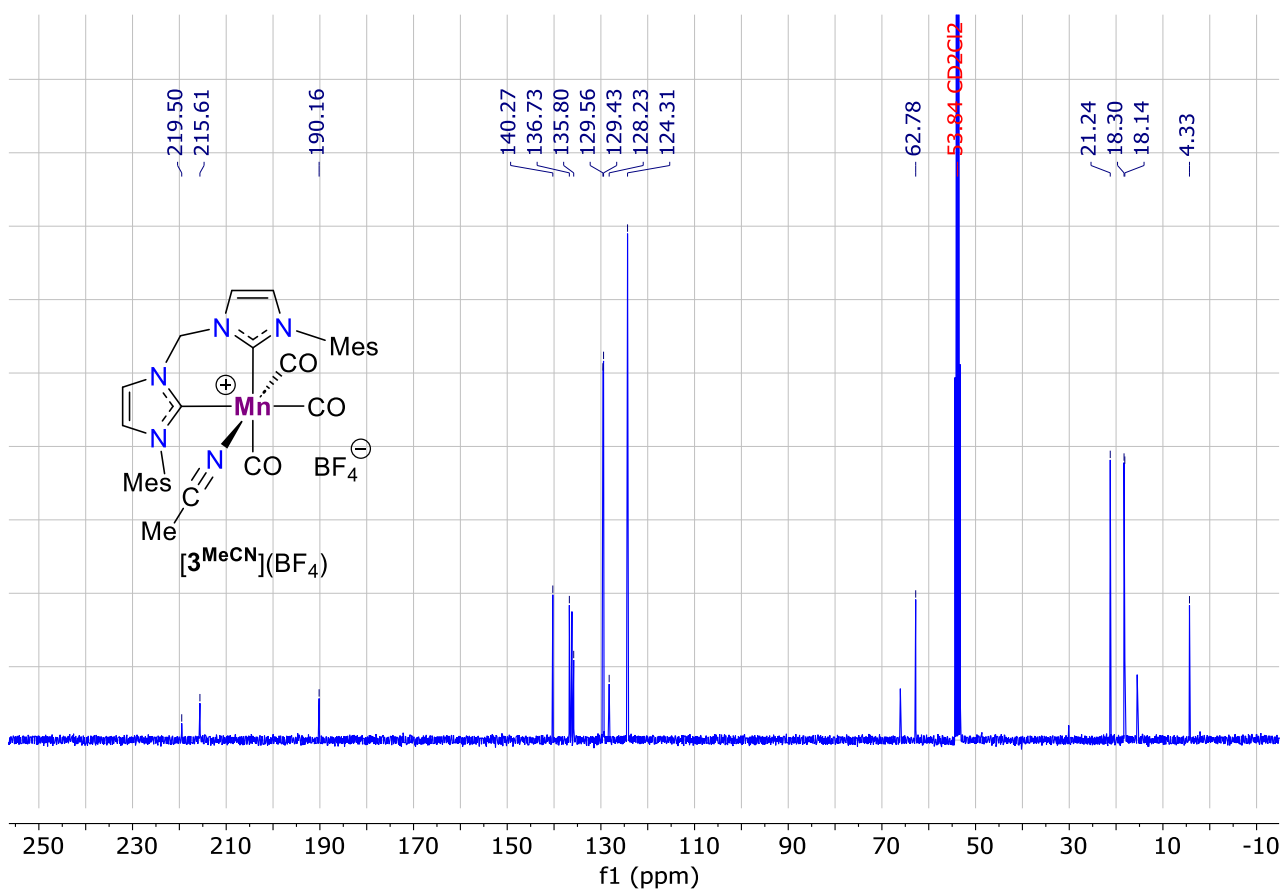


Figure S7. $^{13}C\{^1H\}$ NMR spectrum of complex $[3^{MeCN}](BF_4)$ (100.6 MHz, CD_2Cl_2 , 25°C).

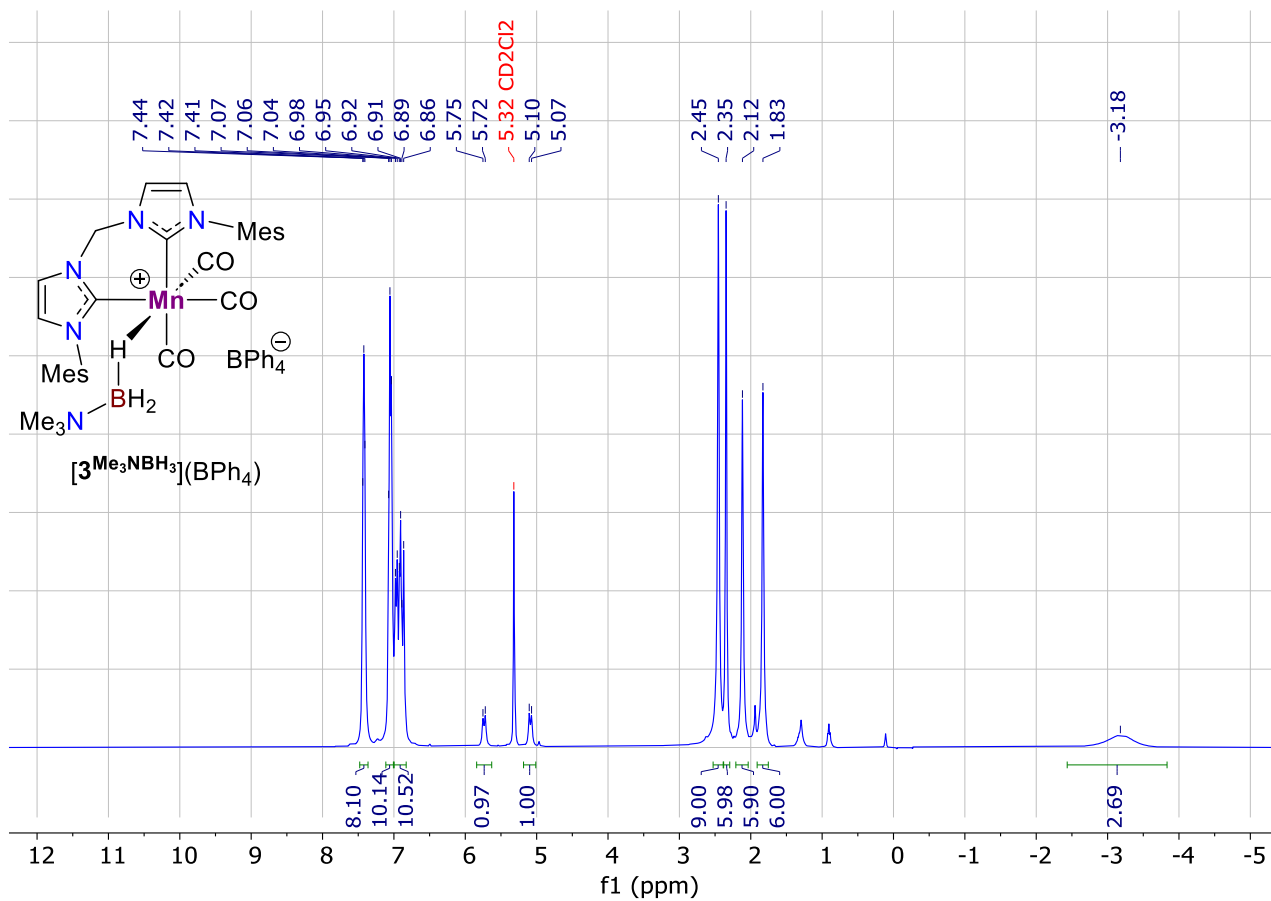


Figure S8. ^1H NMR spectrum of complex $[3\text{Me}_3\text{NBH}_3](\text{BPh}_4)$ (400.1 MHz, CD_2Cl_2 , 25°C).

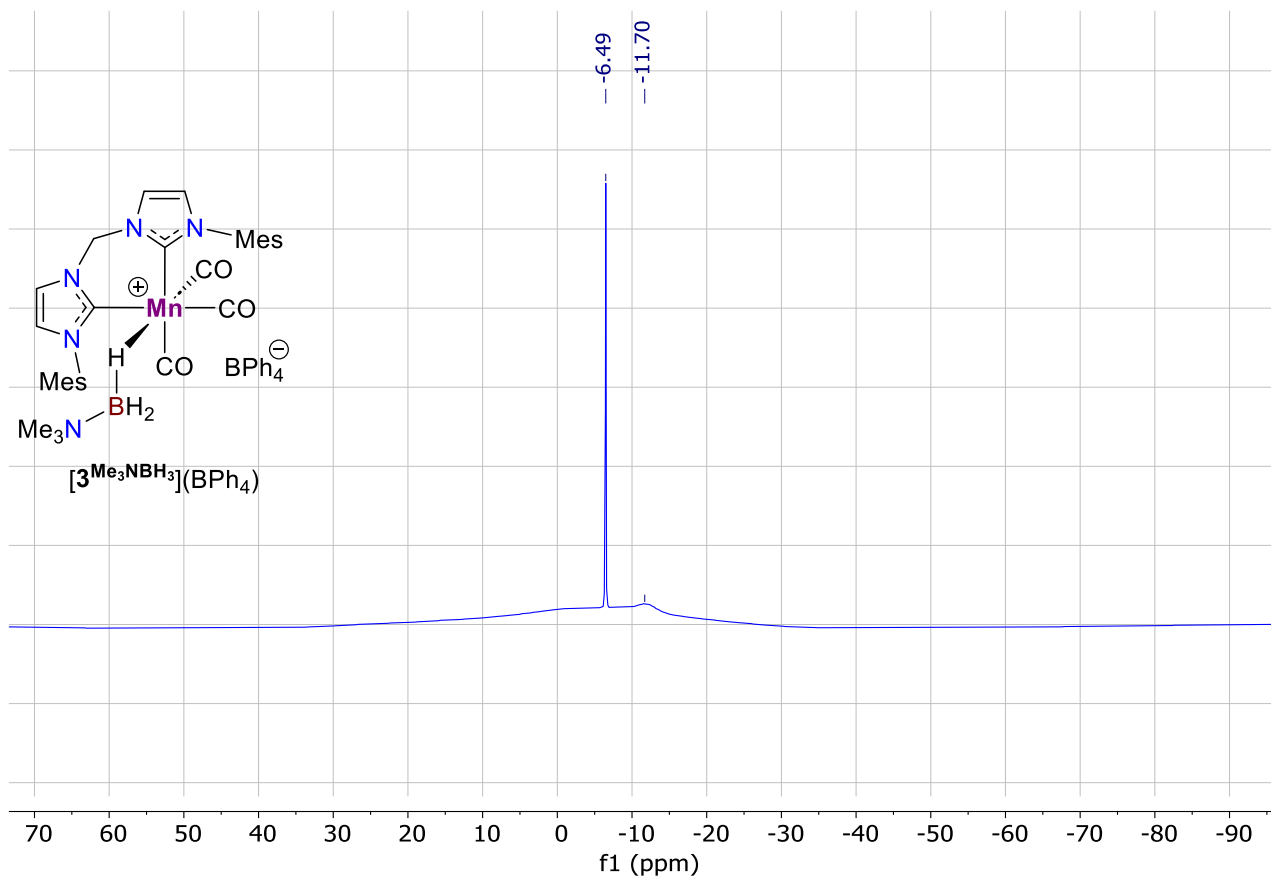


Figure S9. $^{11}\text{B}\{^1\text{H}\}$ NMR spectrum of complex $[3\text{Me}_3\text{NBH}_3](\text{BPh}_4)$ (128.4 MHz, CD_2Cl_2 , 25°C).

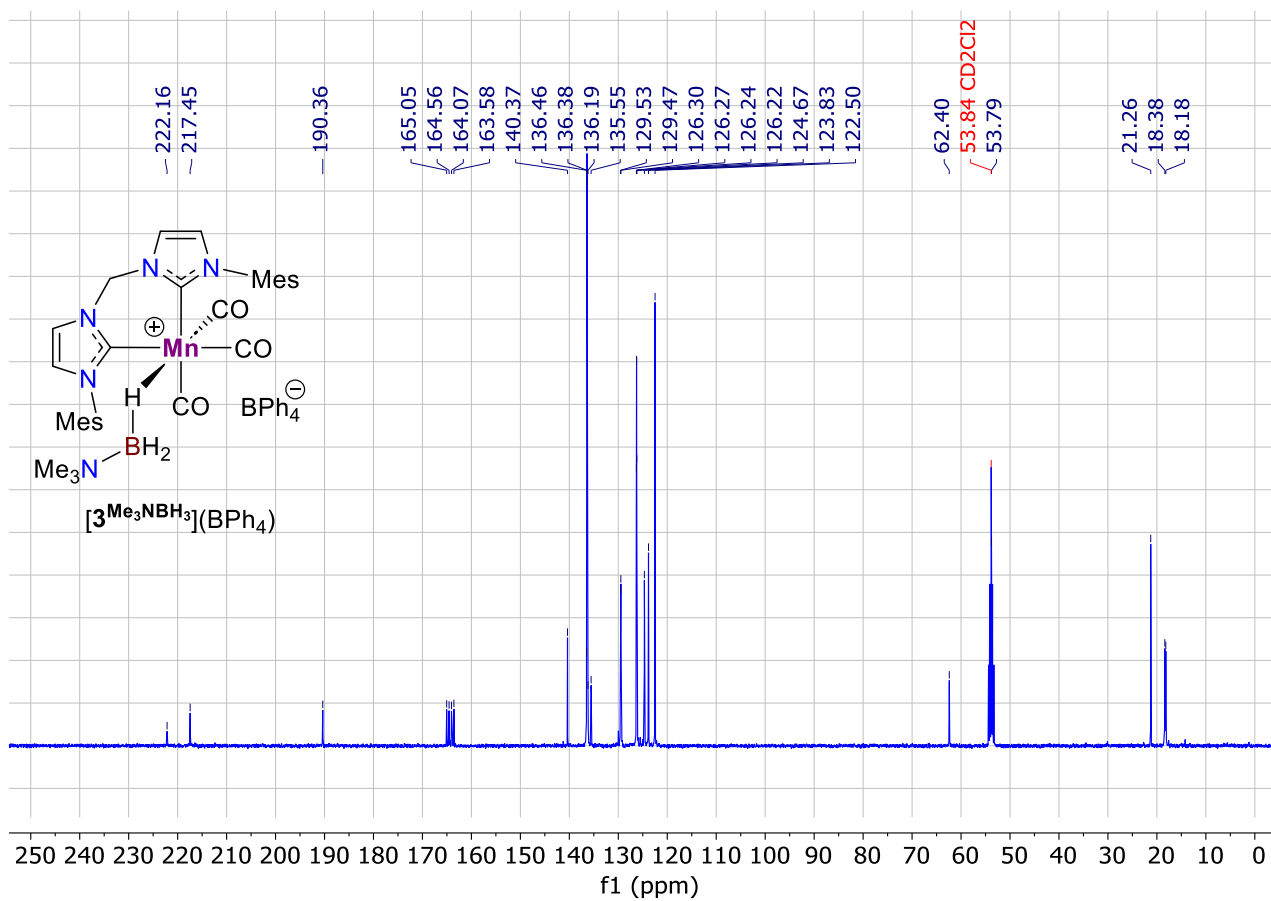


Figure S10. $^{13}\text{C}\{^1\text{H}\}$ NMR spectrum of complex $[\mathbf{3}^{\text{Me}_3\text{NBH}_3}](\text{BPh}_4)$ (100.6 MHz, CD_2Cl_2 , 25°C).

Pressure vs. time studies of amine-boranes dehydrogenation

Hydrogen evolution during dehydrogenation of amine-boranes was monitored in a closed reactor under constant volume conditions using the *Man on the Moon X103* kit (Figure S11, left), device conceived by the University of Zaragoza (Spain) for monitoring the progress of reactions that evolve gases by measuring the pressure variation vs. time (more information about the features of the kit can be found at the following link: <http://www.manonthemoontech.com/x103-gas-evolution.html>).

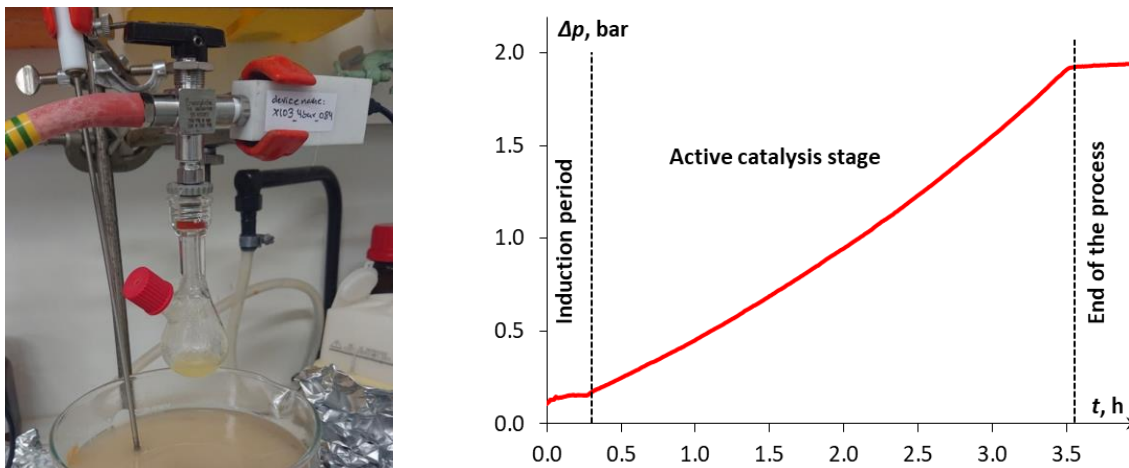


Figure S11. Photo of “*Man on the Moon X103*” device (left) and typical kinetic curve (Δp vs. time) for H_2 production from DMAB dehydrogenation in PhCl (right) catalyzed by complex 3^{Br} in the presence of $NaBPh_4$ showing the induction period due to pre-catalyst activation.

A set of two-necked round-bottom flasks (21, 30, 34, 38 and 72 mL) was utilized with a three-way valve (2 mL). Total volume of the system was 23–74 mL (flask volume + three-way valve). At the beginning of every experiment, the flask was filled with inert gas and connected to a Schlenk line via three-way valve. The solutions with total volume 2 mL were prepared via one of four methods below and the resulting mixture was stirred in an oil-bath at 30–60°C. Data from a pressure sensor connected via a wireless network to a computer were recorded as a function of pressure vs. time for 3–80 hours. The accumulated pressure variation values were referenced by the pressure of the reaction mixture during the induction period (Figure S11, right) or by the solvent pressure in a blank experiment at the given temperature, and used to calculate the H_2 amount evolved (in equivalents) with 10% precision. The calculations were performed in the ideal gas approximation ($pV = nRT$). The induction period (10–20 min) that was excluded for initial hydrogen evolution rate estimation, however was taken into account for full reaction time calculations for TOF values determination.

Method I (in situ generated cationic complexes [1- 3^{BuCl}]($B(C_6F_5)_4$) from Mn(I) hydrides):

Cationic complexes [1- 3^{BuCl}]($B(C_6F_5)_4$) were generated *in situ* by adding [Ph_3C]($B(C_6F_5)_4$) (6.1 mg, 0.0066 mmol,) dissolved in $nBuCl$ (1.5 mL) to solid hydride complexes 1^H – 3^H (0.0060 mmol) inside the flask. The flask was tightly closed with a septum cap, placed into an oil bath preheated at the indicated temperature and the valve was opened to the pressure sensor. When the solution reached the desired temperature and the pressure stopped changing, the three-way valve was turned to Schlenk line, the cap was opened, and the chosen amount of Me_2NHBH_3 (0.15–0.6 mmol, 8.8–35.4 mg) in $nBuCl$ (0.5 mL) was added under an inert gas flow. Then the system was tightly closed with a cap again, and the three-way valve was opened to the pressure sensor.

Method II (isolated cationic complex [3 MeCN](BF_4)): The flask was charged with solid complex [3 MeCN](BF_4) (1.0 mg, 0.0015 mmol,) and Me_2NHBH_3 (88.4 mg, 1.5 mmol). After three vacuum/inert gas filling cycles PhCl (2 mL) was added under an inert gas flow. Then the system was tightly closed with a cap, placed into an oil bath preheated at the indicated temperature, and the three-way valve was opened to the pressure sensor.

Method III (*in situ* generated cationic complexes from solid Mn(I) bromides): The flask was charged with solid complex $1^{\text{Br}}-3^{\text{Br}}$ (0.0015–0.15 mmol), NaBPh_4 (5.1–102.7 mg, 0.015–0.3 mmol,) and selected amine-borane (0.80–1.50 mmol). After three vacuum/inert gas filling cycles 2 mL of required solvent were added through open flask neck in an inert gas flow. Then the system was tightly closed with a cap, placed in an oil bath preheated at the indicated temperature, and the three-way valve was opened to the pressure sensor.

Method IV (*in situ* generated cationic complex from stock solution of Mn(I) bromide in PhCl): In a separate Schlenk flask a 1.5 mM stock solution of 3^{Br} (4.5 mg, 0.0075 mmol in 5 mL of dry solvent) was prepared by sonication during 10 min. The *Man On the Moon* flask was charged with NaBPh_4 (5.1 mg, 0.015 mmol) and selected amine-borane (0.80–3.75 mmol). After three vacuum/inert gas filling cycles PhCl (2 mL) was added through open flask neck in an inert gas flow. Afterwards, the system was tightly closed with a cap, placed into an oil bath preheated at the indicated temperature, and the three-way valve was opened to the pressure sensor. When the solution reached the desired temperature and pressure stopped changing, the three-way valve was turned to Schlenk line, the cap was opened, and the chosen amount of 3^{Br} stock solution ($7.5 \cdot 10^{-5}$ – $3.0 \cdot 10^{-3}$ mmol, 0.050–1.00 mL) was added with a syringe in an inert gas flow.

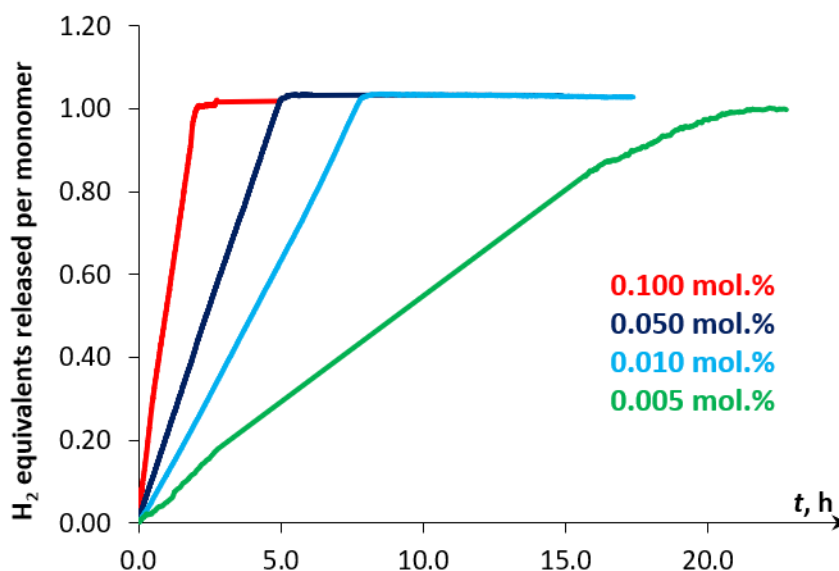


Figure S12. Hydrogen evolution kinetic curves for DMAB dehydrogenation at 60°C using different concentrations of 3^{Br} in the presence of NaBPh_4 (1 mol%).

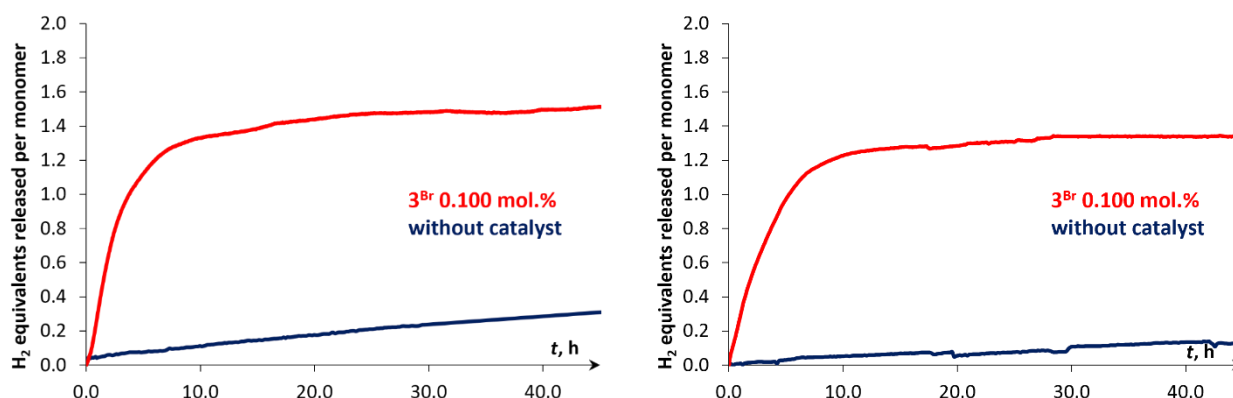


Figure S13. Hydrogen evolution kinetic curves (Δp vs. time) for the dehydrogenation of $t\text{BuNH}_2\text{BH}_3$ (69.6 mg, 0.8 mmol, left) and MeNH_2BH_3 (35.9 mg, 0.8 mmol, right) in PhCl (2 mL) at 60°C catalyzed by complex 3^{Br} (0.1 mol%) in the presence of NaBPh_4 (1 mol%). The corresponding profiles for thermal hydrogenation of these substrates in the absence of manganese catalyst are shown in blue.

Table S1. Additional optimization data for catalytic DMAB dehydrogenation obtained from pressure vs. time experiments.^a

$\text{Me}_2\text{NH}-\text{BH}_3 \xrightarrow[\text{solvent, temperature (}^\circ\text{C)}]{\text{pre-catalyst x mol\%}} \begin{array}{c} \text{Me}_2\text{N}-\text{BH}_2 \\ \quad \\ \text{H}_2\text{B}-\text{NMe}_2 \end{array} + \text{H}_2$									
Entry	[cat]	Additive	Solvent	Catalyst loading (x)	Temperature	TON ^b	TOF ^b ,	H ₂ evolution time (equiv.)	Initial rate, mol·l ⁻¹ ·s ⁻¹
1	-	-	PhCl	-	60°C			NO REACTION ^c	
2	-	NaBPh ₄	PhCl	-	60°C			NO REACTION ^c	
3	1^{Br}	NaBPh ₄	PhCl	10 mol%	50°C	1	<< 1 h ⁻¹	100 h (0.01)	2.2·10 ⁻⁷
4 ^d	[1^{nBuCl}](B(C ₆ F ₅) ₄)	-	nBuCl	4.0 mol%	50°C	25	< 1 h ⁻¹	38.0 h (0.1)	5.0·10 ⁻⁷
5	2^{Br}	NaBPh ₄	PhCl	1.0 mol%	50°C	100	1 h⁻¹	72.0 h (1.00)	4.0·10 ⁻⁶
6 ^d	[2^{nBuCl}](B(C ₆ F ₅) ₄)	-	nBuCl	4.0 mol%	50°C	25	9 h⁻¹	2.8 h (1.00)	1.1·10 ⁻⁵
7 ^e	[3^{nBuCl}](B(C ₆ F ₅) ₄)	-	nBuCl	1.0 mol%	50°C	100	143 h⁻¹	0.7 h (1.00)	2.4·10 ⁻⁴
8	[3^{MeCN}](BF ₄)	-	PhCl	0.1 mol%	50°C	981	38 h⁻¹	26.0 h (0.98)	1.1·10 ⁻⁵
9	3^{Br}	-	PhCl	0.1 mol%	50°C	535	5 h⁻¹	118 h (0.54)	1.7·10 ⁻⁶
10	3^H	-	PhCl	2.0 mol%	50°C	29	<1 h ⁻¹	45.5 h (0.58)	5.7·10 ⁻⁶
11	3^H	-	PhCl	0.1 mol%	50°C	253	4 h⁻¹	69.2 h (0.25)	8.4·10 ⁻⁷
12	3^{Br}	NaBF ₄	PhCl	0.1 mol%	50°C	902	13 h⁻¹	69.3 h (0.90)	5.9·10 ⁻⁶
13	3^{Br}	NaB(C ₆ F ₅) ₄	PhCl	0.1 mol%	50°C	1000	244 h⁻¹	4.1 h (1.00)	5.0·10 ⁻⁵
14	3^{Br}	NaBPh ₄	PhCl	0.1 mol%	50°C	1000	259 h⁻¹	3.9 h (1.00)	5.7·10 ⁻⁵
15	3^{Br}	NaBPh ₄	PhCl	0.02 mol%	50°C	5000	256 h⁻¹	19.5 h (1.00)	1.3·10 ⁻⁵
16	3^{Br}	NaBPh ₄	PhCl	0.01 mol%	50°C	10000	286 h⁻¹	35.0 h (1.00)	7.1·10 ⁻⁶
17	3^{Br}	NaBPh ₄	PhCl	0.005 mol%	50°C	17207	350 h⁻¹	49.2 h (0.86)	5.6·10 ⁻⁶
18 ^f	3^{Br}	NaBPh ₄	PhCl	0.005 mol%	50°C	18318	1047 h⁻¹	16 h (0.92)	1.3·10 ⁻⁵
19	3^{Br}	NaBPh ₄	PhCl	0.1 mol%	60°C	1000	476 h⁻¹	2.1 h (1.00)	1.1·10 ⁻⁴
20 ^f	3^{Br}	NaBPh ₄	PhCl	0.1 mol%	60°C	1000	625 h⁻¹	1.6 h (1.00)	1.3·10 ⁻⁴
21 ^g	3^{Br}	NaBPh ₄	PhCl	0.1 mol%	60°C	254	4 h⁻¹	60.0 h (0.25)	8.4·10 ⁻⁷
22	3^{Br}	NaBPh ₄	PhCl	0.02 mol%	60°C	5000	1058 h⁻¹	4.8 h (1.00)	4.6·10 ⁻⁵
23	3^{Br}	NaBPh ₄	PhCl	0.01 mol%	60°C	10000	1157 h⁻¹	8.7 h (1.00)	2.7·10 ⁻⁵
24	3^{Br}	NaBPh ₄	PhCl	0.005 mol%	60°C	16221	661 h⁻¹	24.6 h (0.81)	1.3·10 ⁻⁵
25 ^f	3^{Br}	NaBPh ₄	PhCl	0.005 mol%	60°C	18242	1267 h⁻¹	14.4 h (0.99)	2.0·10 ⁻⁵
26	3^{Br}	NaBPh ₄	PhCl	0.1 mol%	30°C	1000	56 h⁻¹	17.7 h (1.00)	1.1·10 ⁻⁵
27	3^{Br}	NaBPh ₄	PhCl	0.1 mol%	35°C	1000	74 h⁻¹	13.6 h (1.00)	1.7·10 ⁻⁵
28	3^{Br}	NaBPh ₄	PhCl	0.1 mol%	40°C	1000	94 h⁻¹	10.6 h (1.00)	2.5·10 ⁻⁵
29	3^{Br}	NaBPh ₄	PhCl	0.1 mol%	45°C	1000	179 h⁻¹	5.6 h (1.00)	3.9·10 ⁻⁵
30	3^{Br}	NaBPh ₄	PhCl	0.1 mol%	55°C	1000	385 h⁻¹	2.6 h (1.00)	7.0·10 ⁻⁵
31	3^{Br}	NaBPh ₄	PhF	0.1 mol%	50°C	1000	149 h⁻¹	6.7 h (1.00)	2.9·10 ⁻⁵
32	3^{Br}	NaBPh ₄	THF	0.1 mol%	50°C	1000	38 h⁻¹	26.0 h (1.00)	7.6·10 ⁻⁶
33	3^{Br}	NaBPh ₄	DMF	0.1 mol%	50°C	88	5 h⁻¹	19.0 h (0.09)	8.1·10 ⁻⁷

^a $n(\text{Me}_2\text{NHBH}_3) = 1.5 \text{ mmol}$; ^b average from two independent runs estimated from the volume of released H₂; ^c no changes in pressure were detected in the system in more than 20 h; ^d $n(\text{Me}_2\text{NHBH}_3) = 0.16 \text{ mmol}$; ^e $n(\text{Me}_2\text{NHBH}_3) = 0.64 \text{ mmol}$; ^f reaction was performed in the dark; ^g reaction was performed in air atmosphere

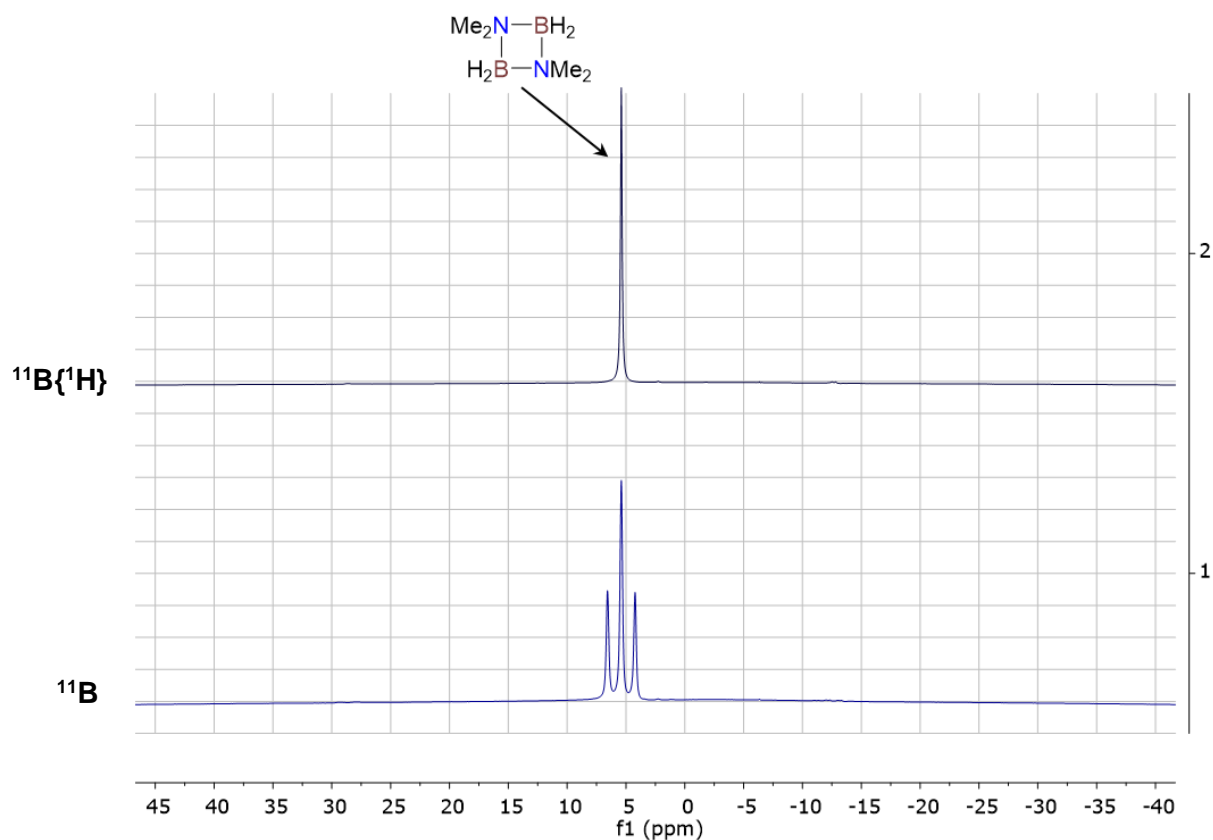


Figure S14. ^{11}B and $^{11}\text{B}\{^1\text{H}\}$ NMR spectra (128.3 MHz, $\text{PhCl}/\text{C}_6\text{D}_6$, 25°C) of crude products obtained from DMAB dehydrogenation in dark at 60°C catalyzed by 3^{Br} (0.005 mol.%) and NaBPh_4 (1.0 mol.%).

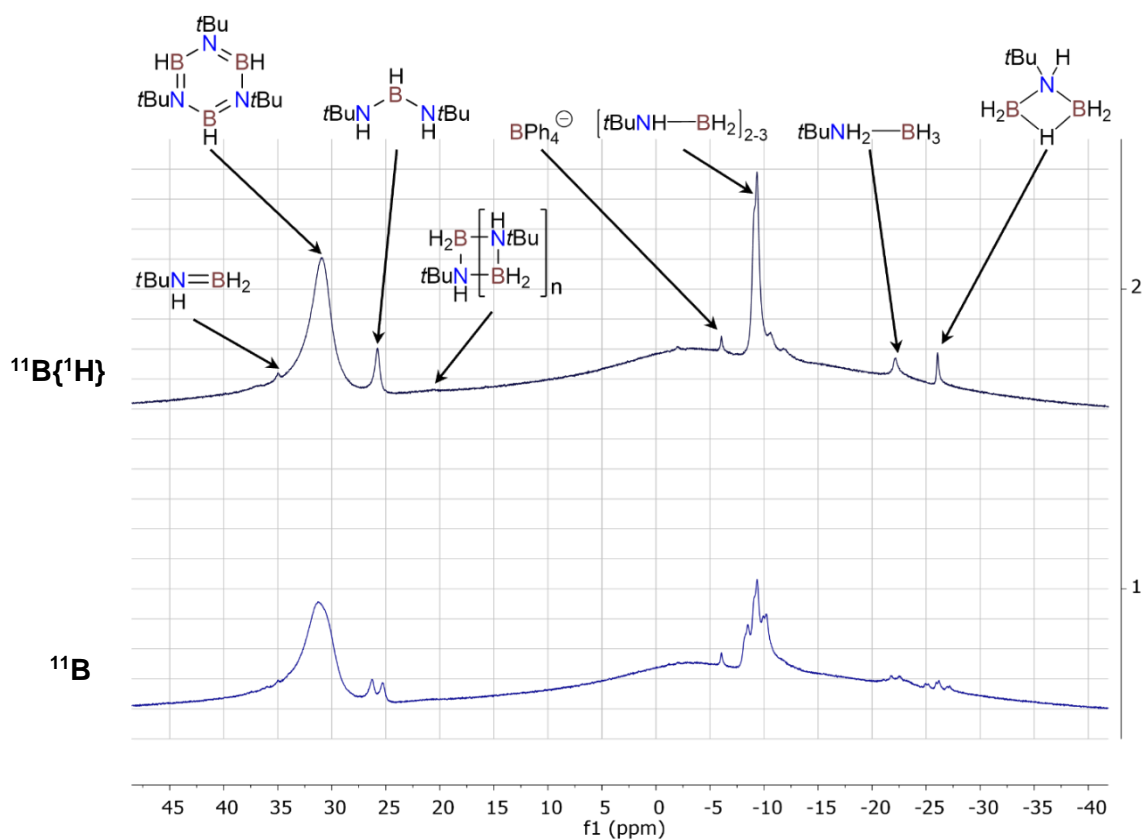


Figure S15. ^{11}B and $^{11}\text{B}\{^1\text{H}\}$ NMR spectra (128.3 MHz, $\text{PhCl}/\text{C}_6\text{D}_6$, 25°C) of crude products obtained from $t\text{BuNH}_2\text{BH}_3$ dehydrogenation at 60°C catalyzed by 3^{Br} (0.1 mol.%) and NaBPh_4 (1.0 mol.%).

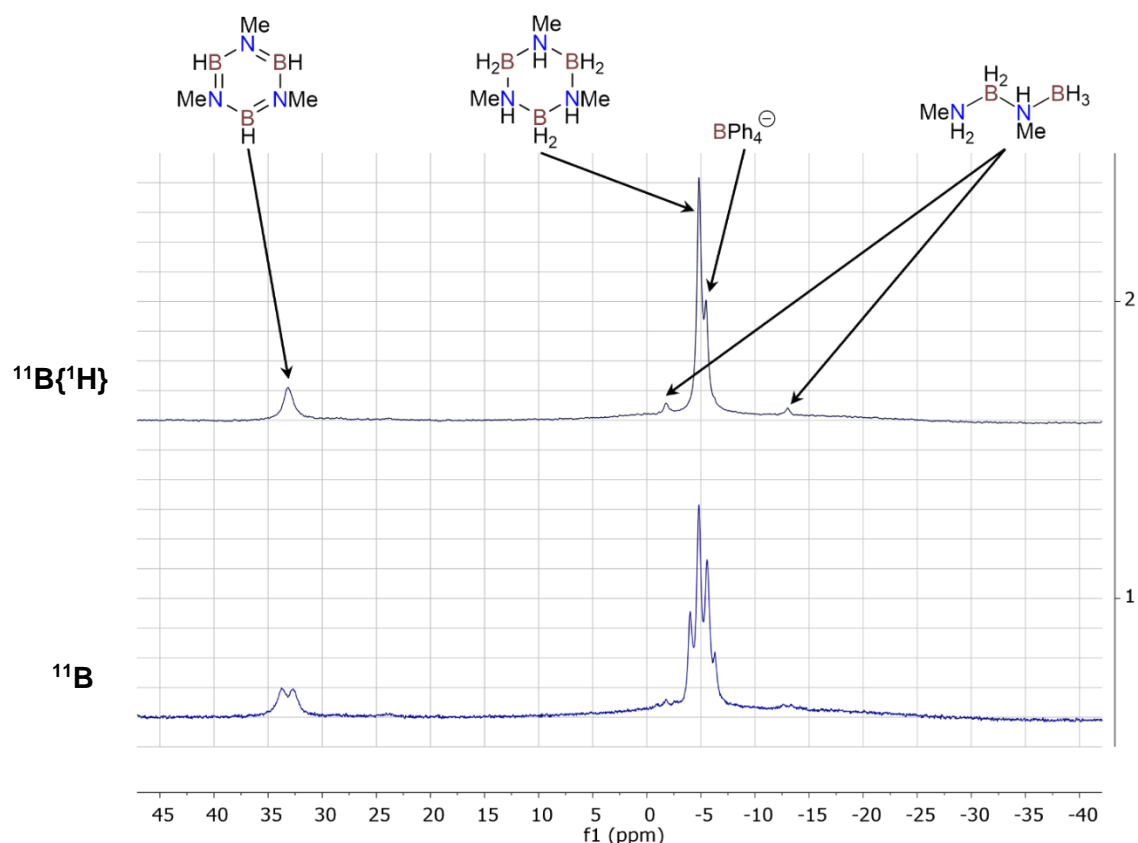


Figure S16. ^{11}B and $^{11}\text{B}\{^1\text{H}\}$ NMR spectra (128.3 MHz, PhCl/ C_6D_6 , 25°C) of crude products obtained from MeNH_2BH_3 dehydrogenation at 60°C catalyzed by 3^{Br} (0.1 mol.%) and NaBPh_4 (1.0 mol.%).

Table S2. Experimental ^{11}B NMR data (128.3 MHz, 25°C) for DMAB and its dehydrogenation products in CH_2Cl_2 and PhCl

Compound	δ_{BH} , ppm	
	PhCl (C_6D_6 capillary)	CD_2Cl_2
$\text{Me}_2\text{NH}-\text{BH}_3$	-13.5 (q, $^1J_{\text{BH}} = 96.1$ Hz)	-13.8 (q, $^1J_{\text{BH}} = 96.1$ Hz)
$\text{Me}_2\text{N}-\text{BH}_2$ $\text{H}_2\text{B}-\text{NMe}_2$	5.3 (t, $^1J_{\text{BH}} = 112.8$ Hz)	5.2 (t, $^1J_{\text{BH}} = 112.1$ Hz)
$\text{Me}_2\text{N}=\text{BH}_2$	37.9 (t, $^1J_{\text{BH}} = 128.8$ Hz)	37.5 (t, $^1J_{\text{BH}} = 128.2$ Hz)
$\text{Me}_2\text{N}-\text{B}(\text{H})-\text{NMe}_2$	28.7 (d, $^1J_{\text{BH}} = 130.9$ Hz)	28.6 (d, $^1J_{\text{BH}} = 131.0$ Hz)
$\text{H}_3\text{B}-\text{N}(\text{Me}_2)-\text{B}(\text{H}_2)-\text{NHMe}_2$	2.1 (t, $^1J_{\text{BH}} = 110.1$ Hz, BH_2), -13.0 (q, 94.0 Hz, BH_3)	2.2 (t, $^1J_{\text{BH}} = 110.3$ Hz, BH_2), -13.5 (q overlapped with signal of DMAB, BH_3)
$\text{H}_2\text{B}-\text{N}(\text{Me}_2)-\text{BH}_2$	-17.5 (td, $^1J_{\text{BH}} = 129.4, 32.2$ Hz)	-17.6 (td, $^1J_{\text{BH}} = 128.0$ Hz, 32.2 Hz)
$\text{B}(\text{OH})_3$	20.8 (br. s)	20.9 (br. s)

Table S3. Experimental ^{11}B NMR data (128.3 MHz, 25°C, PhCl/ C_6D_6) for $t\text{BuNH}_2\text{BH}_3$ and its dehydrogenation products.

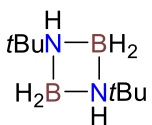
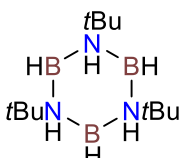
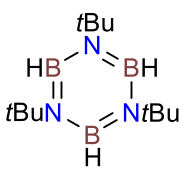
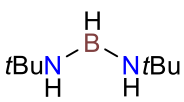
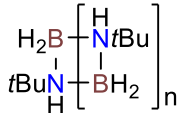
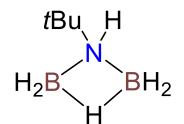
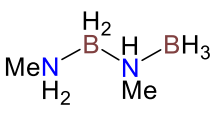
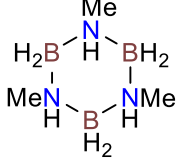
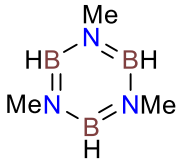
Compound	δ_{B} ppm (PhCl with C_6D_6 capillary)
$t\text{BuNH}_2\text{—BH}_3$	-22.1 (q, $^1J_{\text{BH}} = 95.3$ Hz)
	-9.1 (t overlapped with t of $(t\text{BuNHBH}_2)_3$, $^1J_{\text{BH}} = 112.4$ Hz)
	-9.4 (t overlapped with t of $(t\text{BuNHBH}_2)_2$, $^1J_{\text{BH}} = 112.4$ Hz)
	30.9 (br s)
$t\text{BuN}=\text{BH}_2$	35.0 (t, $^1J_{\text{BH}} = 127.5$ Hz)
	25.9 (d, $^1J_{\text{BH}} = 129.2$ Hz)
	20.5 (br s)
	-26.1 (td, $^1J_{\text{BH}} = 127.1$ Hz, 33.3 Hz)

Table S4. Experimental ^{11}B NMR data (128.3 MHz, 25°C, PhCl/ C_6D_6) for MeNH_2BH_3 and its dehydrogenation products.

Compound	δ_{B} ppm (PhCl with C_6D_6 capillary)
$\text{MeNH}_2\text{—BH}_3$	-17.5 (q, $^1J_{\text{BH}} = 96.4$ Hz)
	-1.8 (t, $^1J_{\text{BH}} = 104.2$ Hz, BH_2), -13.0 (q, 94.5 Hz, BH_3)
	-4.8 (t, $^1J_{\text{BH}} = 102.4$ Hz)
	33.2 (d, $^1J_{\text{BH}} = 140.0$ Hz)

General procedure for IR monitoring.

The solution of 3^{Br} (12.2 mg, 0.01 mmol) was prepared at room temperature in 1 mL of CH_2Cl_2 or PhCl , and then an aliquot was taken with a Pasteur pipette and placed in the inert gas filled cell ($l = 0.01\text{--}0.1$ cm). After the reference IR spectrum of initial bromide complex 3^{Br} was acquired, the sample was returned into the Schlenk tube. In a separate Schlenk tube a mixture of NaBPh_4 (45.0 mg, 0.13 mmol,) and Me_2NHBH_3 (32.0 mg, 0.30 mmol) was prepared under inert atmosphere. To this solid mixture the initial solution of 3^{Br} was added in an inert gas flow. Obtained suspension was quickly mixed under sonication and an aliquot was transferred in the inert gas filled cell for IR monitoring at room temperature.

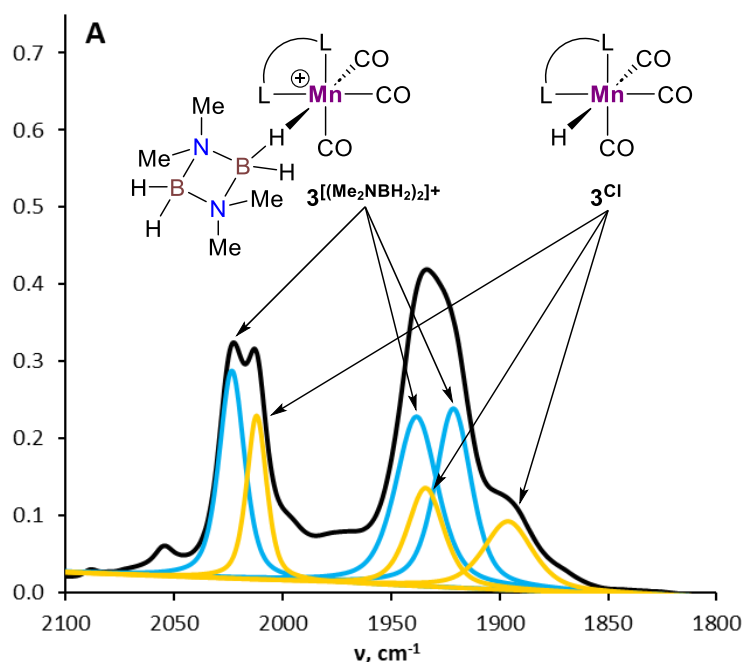


Figure S17. Bands decomposition for the IR spectrum obtained at the end of DMAB (32.0 mg, 0.60 mmol) dehydrogenation catalyzed by 3^{Br} (3.3 mol.%) and NaBPh_4 (16.5 mol.%) in CH_2Cl_2 at 30°C ; $l = 0.01$ cm; L = NHC.

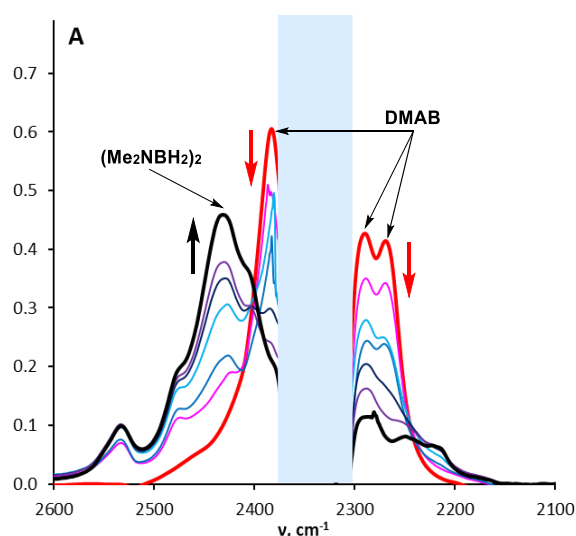


Figure S18. IR spectroscopy monitoring in ν_{BH} range for DMAB (32.0 mg, 0.60 mmol) dehydrogenation by 3^{Br} (3.3 mol.%) and NaBPh_4 (16.5 mol.%) in CH_2Cl_2 at 30°C ; $l = 0.01$ cm; L = NHC. Reaction mixture after addition of Me_2NHBH_3 ($c = 0.15$ M): 2 min. (red), 20 min. (black). The area hidden by the solvent absorption is shaded by light blue.

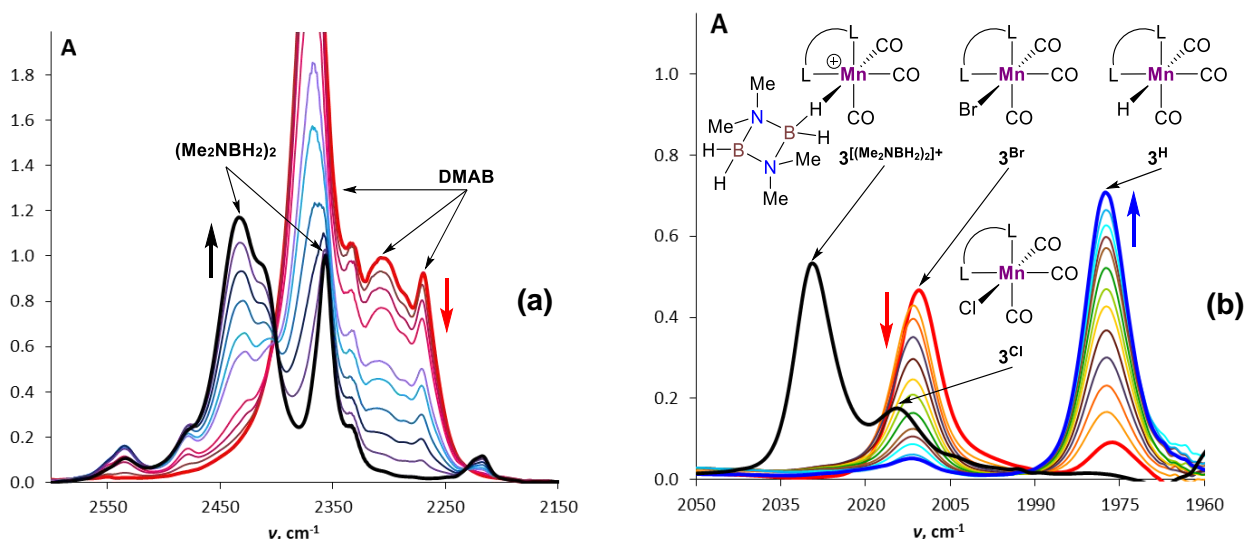


Figure S19. IR spectroscopy monitoring for DMAB ($c = 0.09$ M; 10.6 mg, 0.18 mmol) dehydrogenation by 3^{Br} (3.3 mol.%) and NaBPh_4 (16.5 mol.%) in PhCl at 30°C ; $l = 0.1$ cm; L = NHC. **(a)** in ν_{BH} range. Reaction mixture after addition of Me_2NHBH_3 : 2 min. (red), 120 min. (black); **(b)** in ν_{CO} range. Reaction mixture after addition of Me_2NHBH_3 : 2 min. (red), 55 min. (blue), 120 min. (black).

Table S5. Experimental ν_{CO} frequencies with relative intensities for Mn(I) complexes in PhCl and CH_2Cl_2 .

Complex	$\nu_{\text{CO}}, \text{cm}^{-1}$	
	PhCl	CH_2Cl_2
3^{Br}	2010 (s), 1932 (s), 1895 (s)	2012 (s), 1928 (s), 1892 (s)
3^{Cl}	2013 (s)	2012 (s), 1934 (s), 1896 (s)
3^{H}	1978 (s), 1885 (s)	1975 (s), 1879 (s), 1869 (s)
$3^{\text{[DMAB]}}/3^{\text{[(Me}_2\text{NBH}_3)_2]^+}$	2029 (s), 1902 (s)	2023 (s), 1939 (s), 1925 (s)

General procedure for NMR monitoring.

The solution of $\mathbf{3}^{\text{Br}}$ (1.8–6.1 mg, 0.003–0.010 mmol) was prepared at room temperature ($\sim 25^\circ\text{C}$) in 0.5 mL of CD_2Cl_2 or PhCl (with C_6D_6 in a glass capillary) and transferred to NMR tube containing a mixture of NaBPh_4 (10.0 mg, 0.03 mmol) and Me_2NHBH_3 (18.0 mg, 0.30 mmol) under inert atmosphere. To avoid an excess pressure inside the NMR tube due to H_2 evolution, a thin glass capillary was put through the septum cap allowing H_2 release to the atmosphere. The resulting suspension was quickly mixed under sonication, and the tube was placed into NMR spectrometer to monitor the reaction mixture at 25°C . Selected NMR signals of complexes $\mathbf{3}^{\text{H}}$ and $[\mathbf{3}^{\text{DMAB}}](\text{BPh}_4)$ attributed by an analogy to those of characterized $[\mathbf{3}^{\text{Me}_2\text{NBH}_3}](\text{BPh}_4)$ are given below.

$[\mathbf{3}^{\text{DMAB}}](\text{BPh}_4)$: ^1H NMR (400.1 MHz, CD_2Cl_2 , 25°C): δ 5.69 (d, $^2J_{\text{HH}} = 13.0$ Hz, NCH_2N), 5.51 (d, $^2J_{\text{HH}} = 13.3$ Hz, NCH_2N), 2.91–1.80 ($\text{N}(\text{CH}_3)_2$ and CH_3_{Mes} overlapped with signals of DMAB), -3.37 (br. s, BH_3). $^{13}\text{C}\{^1\text{H}\}$ NMR (100.6 MHz, CD_2Cl_2 , 25°C): δ 218.6, 217.8 (s, $\text{Mn}-\text{CO}$), 191.6 (s, $\text{Mn}-\text{CN}_2$), 140.5 (s, $\text{C}-\text{Me}_{\text{Mes}}$), 136.6 (s, $\text{C}-\text{Me}_{\text{Mes}}$), 136.2 (s, $\text{C}-\text{Me}_{\text{Mes}}$), 135.7 (s, $\text{C}_{\text{ipso Mes}}$), 129.6 (s, CH_{Mes}), 124.8, 123.8 (s, $\text{CH}_{\text{Im-4,5}}$), 62.9 (s, NCH_2N), 21.4 (s, CH_3_{Mes}), 18.5 (s, CH_3_{Mes}), 18.3 (s, CH_3_{Mes}).

$\mathbf{3}^{\text{H}}$: ^1H NMR (400.1 MHz, CD_2Cl_2 , 25°C): δ 5.54 (d, $^2J_{\text{HH}} = 13.0$ Hz, NCH_2N), 5.20 (d, $^2J_{\text{HH}} = 12.9$ Hz, NCH_2N), -7.03 (s, $\text{Mn}-\text{H}$).

$\mathbf{3}^{\text{H}}$: ^1H NMR (400.1 MHz, PhCl/ C_6D_6 , 25°C): -6.80 (s, $\text{Mn}-\text{H}$).

$[\mathbf{3}^{\text{Me}_2\text{NBH}_2}](\text{BPh}_4)$: ^1H NMR (400.1 MHz, PhCl/ C_6D_6 , 25°C): δ -3.30 (br. s, BH_3).

Me_2NHBH_3 (DMAB): ^1H NMR (400.1 MHz, CD_2Cl_2 , 25°C): δ 3.91 (br. s, 1H, NH), 2.49 (s, 6H, $\text{N}(\text{CH}_3)_2$), 1.46 (q overlapping with signal of $\text{N}(\text{CH}_3)_2$ moiety, $^2J_{\text{HH}} = 91.5$ Hz, 3H, BH_3). ^{11}B NMR (128.3 MHz, CD_2Cl_2 , 25°C): δ -13.8 (q, $^1J_{\text{BH}} = 96.1$ Hz, BH_3). $^{13}\text{C}\{^1\text{H}\}$ NMR (100.6 MHz, CD_2Cl_2 , 25°C): δ 44.9 (s, $\text{N}(\text{CH}_3)_2$).

^1H NMR (400.1 MHz, PhCl/ C_6D_6 , 25°C): δ 3.80 (br. s, 1H, NH), 2.08 (s, 6H, $\text{N}(\text{CH}_3)_2$), 1.46 (q, $^2J_{\text{HH}} = 97.3$ Hz, 3H, BH_3 , DMAB, signals are overlapping with signal of $\text{N}(\text{CH}_3)_2$ moiety). ^{11}B NMR (128.3 MHz, PhCl/ C_6D_6 , 25°C): δ -13.5 (q, $^1J_{\text{BH}} = 96.1$ Hz, BH_3).

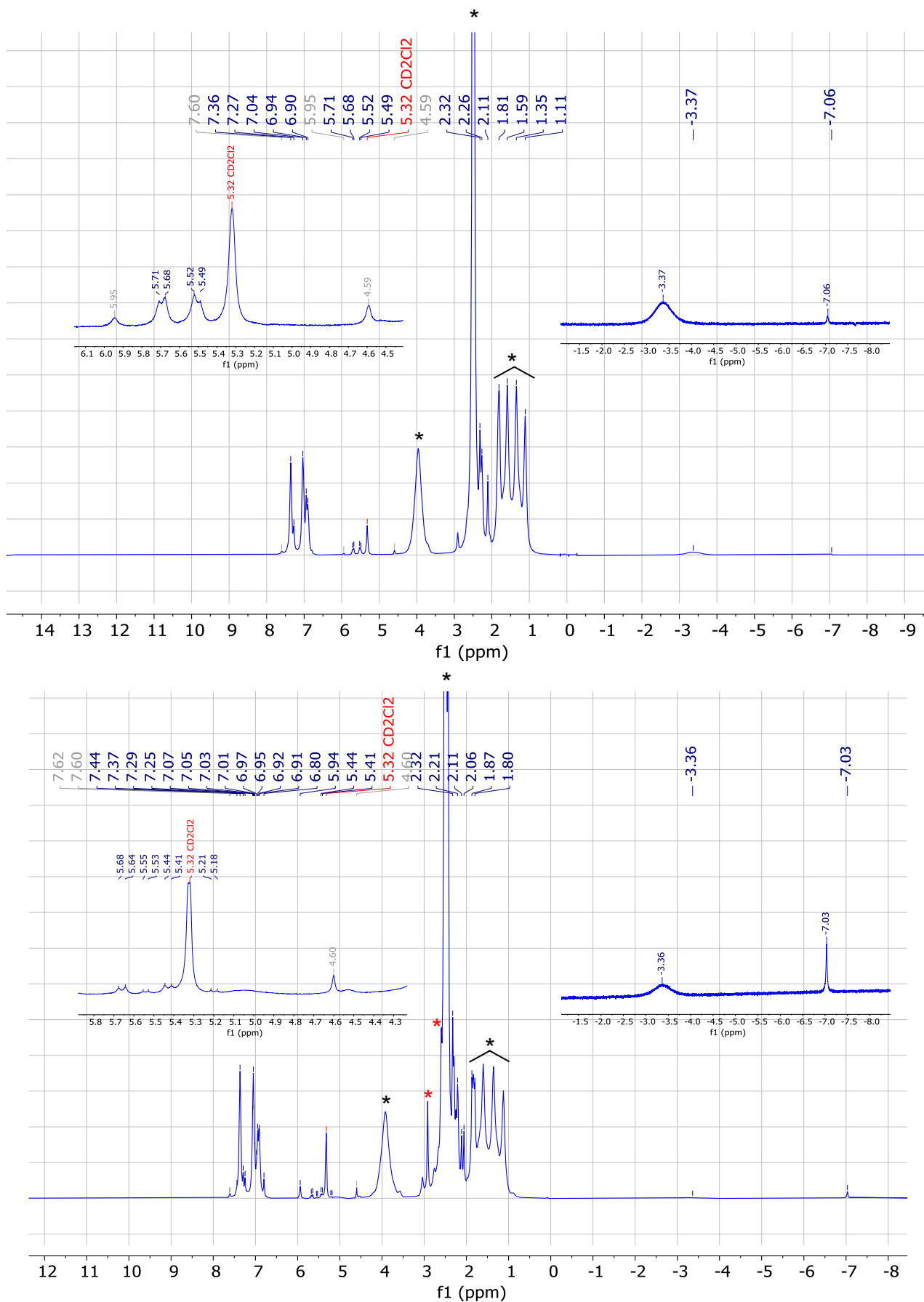


Figure S20. ¹H NMR spectrum (400.1 MHz, CD₂Cl₂, 25°C) of the solution of **3**^{Br} (0.01 mmol, 3.3 mol.%), NaBPh₄ (0.03 mmol, 10 mol.%), and DMAB (0.3 mmol) in CD₂Cl₂ after 15 min (top) and 120 min (bottom) of reaction time. L = NHC. The signals of Me₂NHBH₃ and ((Me₂NBH₂)₂) are marked with black (*) and red (*) asterisk, respectively.

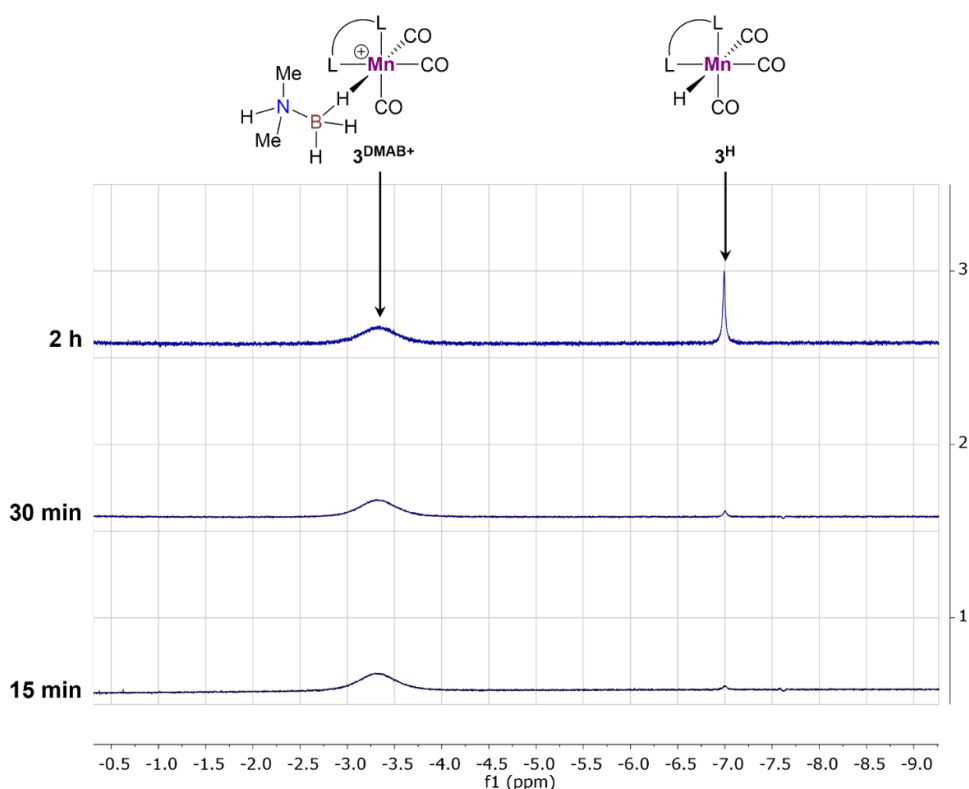


Figure S21. ^1H NMR monitoring (400.1 MHz, CD_2Cl_2 , 25°C) of DMAB (0.3 mmol) dehydrogenation catalyzed by 3^{Br} (0.01 mmol, 3.3 mol.%) and NaBPh_4 (0.03 mmol, 10 mol.%) in CD_2Cl_2 ; L = NHC.

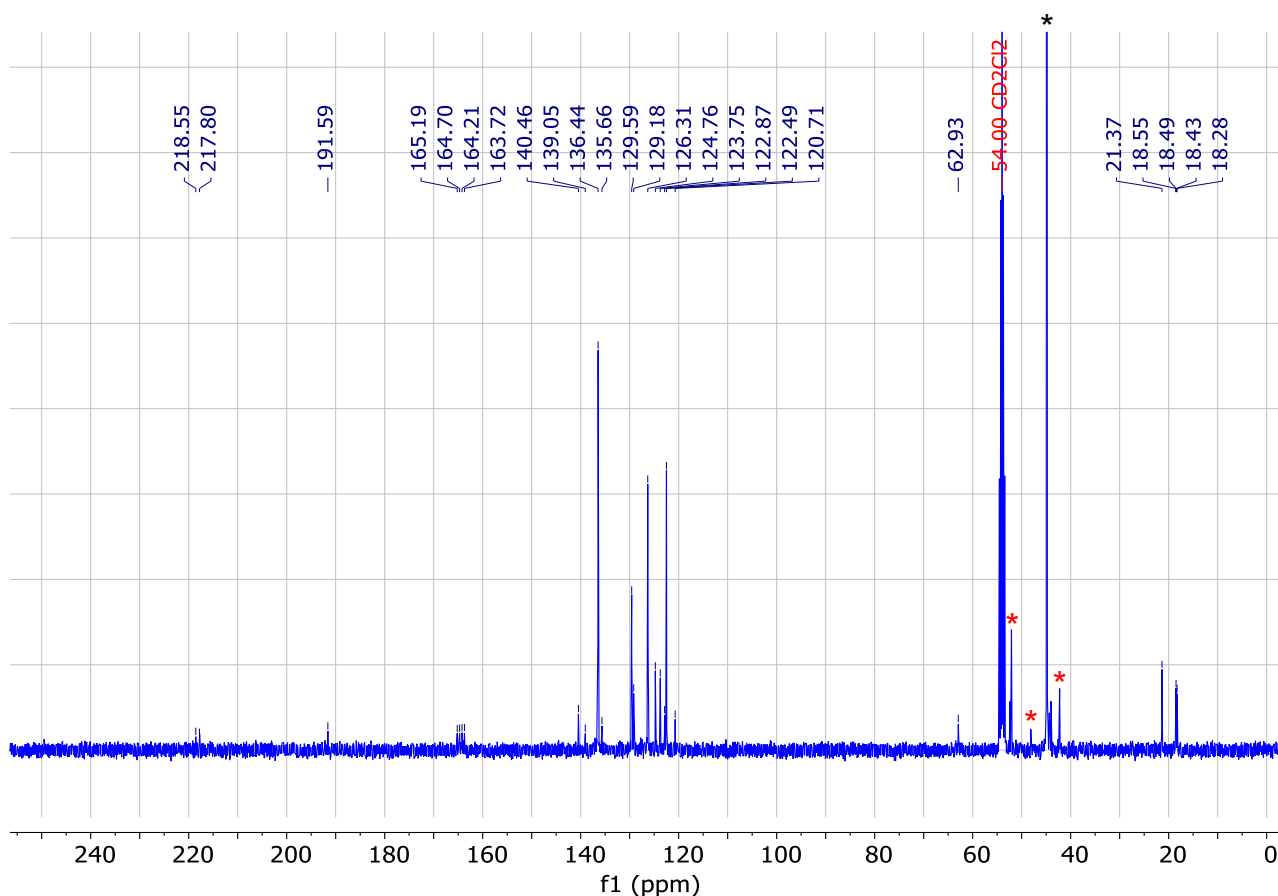


Figure S22. $^{13}\text{C}\{^1\text{H}\}$ NMR spectrum (100.6 MHz, CD_2Cl_2 , 25°C) of the solution of 3^{Br} (0.01 mmol, 3.3 mol.%), NaBPh_4 (0.03 mmol, 10 mol.%), and Me_2NHBH_3 (0.3 mmol) in CD_2Cl_2 after 45 min. L = NHC. The signals of methyl groups in Me_2NHBH_3 and its dehydrogenation intermediates/products are marked with black (*) and red (*) asterisks, respectively.

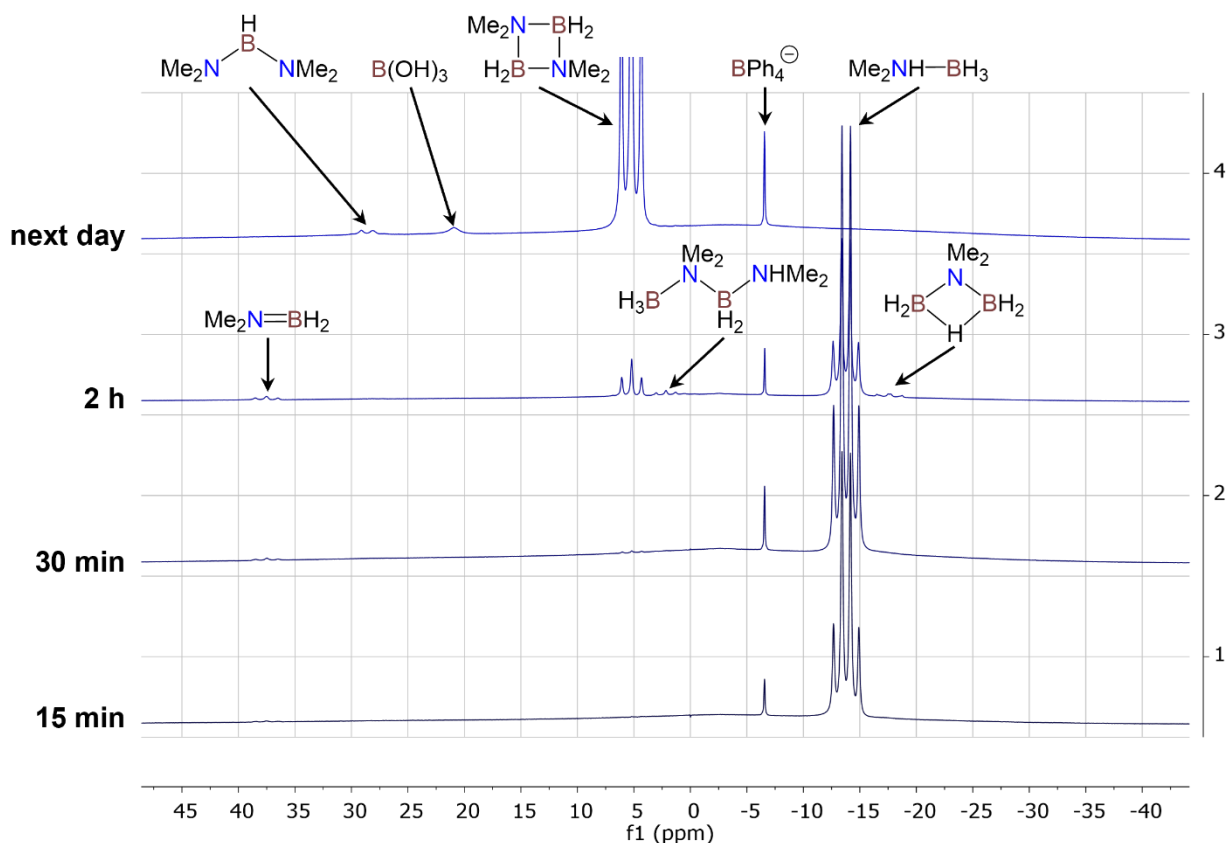


Figure S23. ^{11}B NMR monitoring (128.3 MHz, CD_2Cl_2 , 25°C) of Me_2NHBH_3 ($c = 0.6$ M) dehydrogenation catalyzed by $\mathbf{3}^{\text{Br}}$ ($c = 0.02$ M, 3.3 mol.%) and NaBPh_4 (16.5 mol.%).

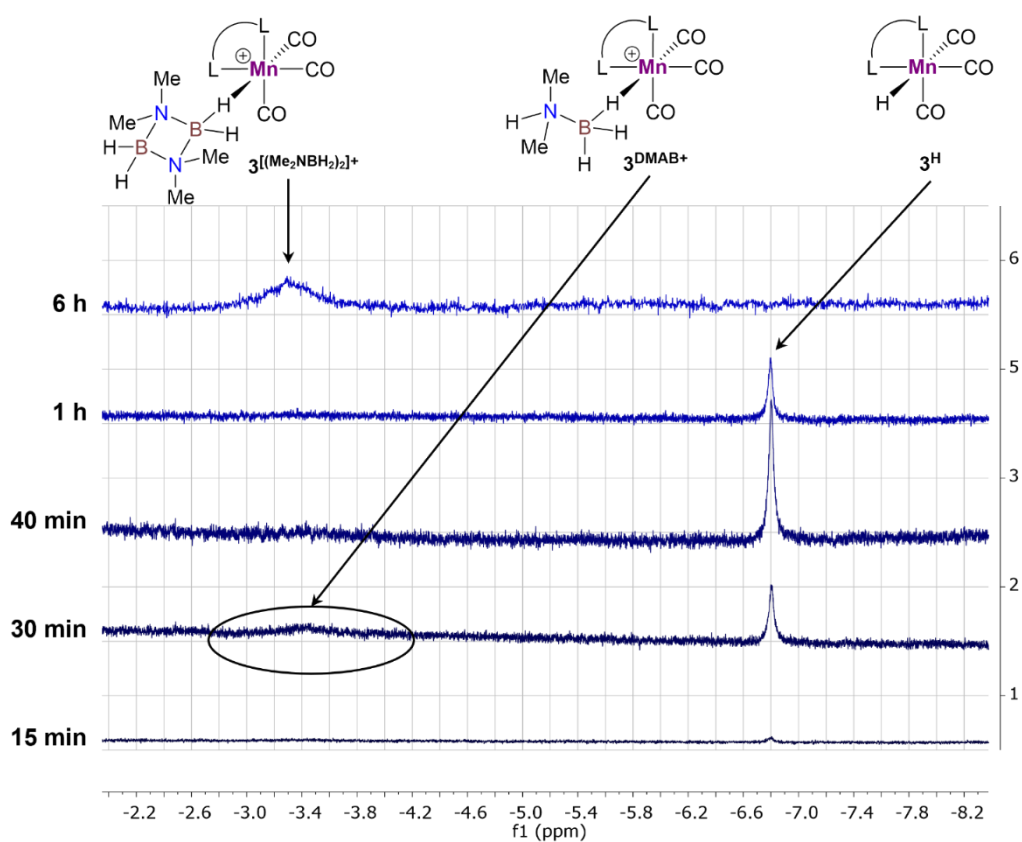


Figure S24. ^1H NMR monitoring (400.1 MHz, $\text{PhCl}/\text{C}_6\text{D}_6$, 25°C) of Me_2NHBH_3 ($c = 0.6$ M) dehydrogenation catalyzed by $\mathbf{3}^{\text{Br}}$ (0.003 mmol, 1.0 mol.%) and NaBPh_4 (0.015 mmol, 5.0 mol.%). L = NHC.

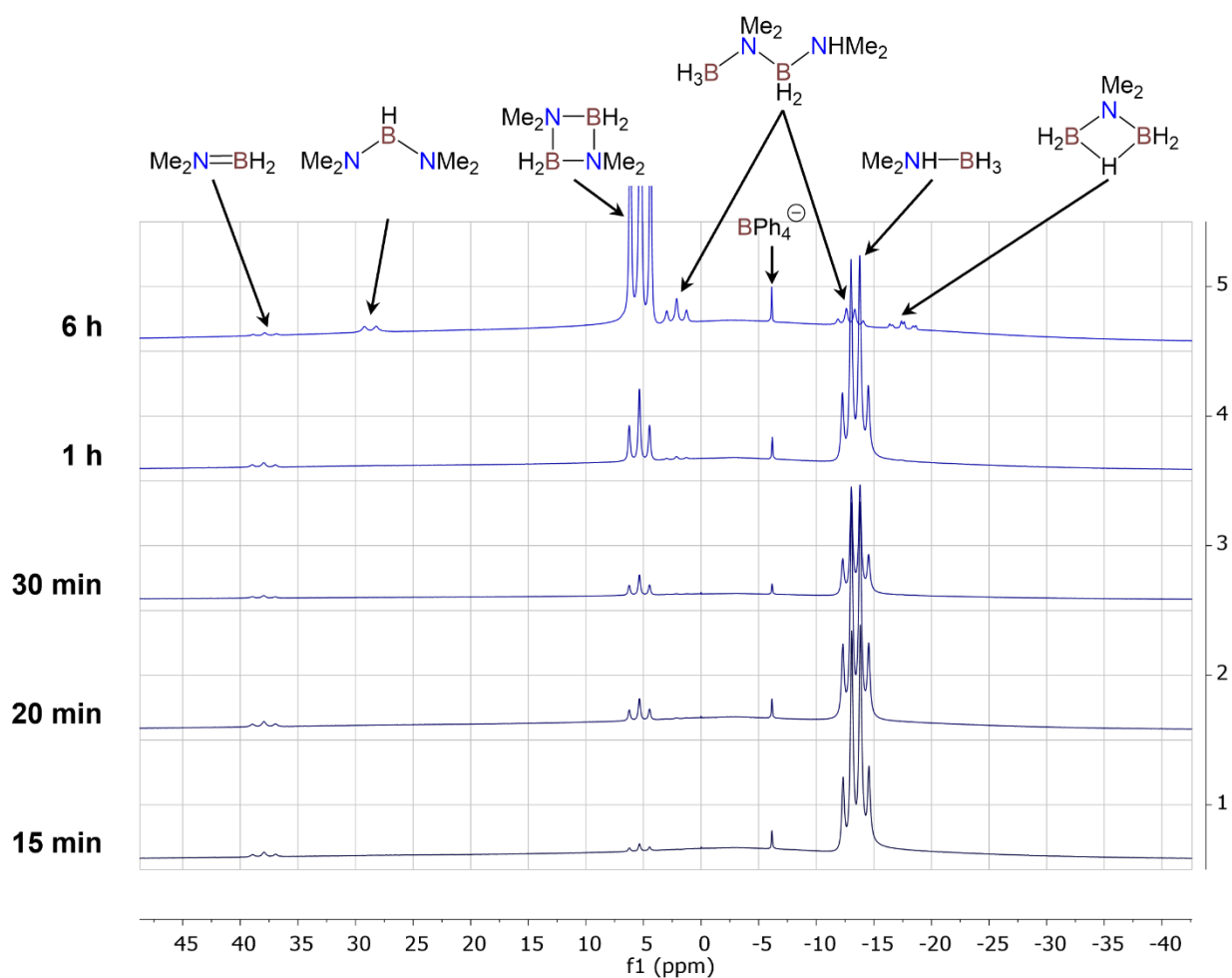


Figure S25. ^{11}B NMR monitoring (128.3 MHz, $\text{PhCl}/\text{C}_6\text{D}_6$, 25°C) of Me_2NHBH_3 ($c = 0.6 \text{ M}$) dehydrogenation catalyzed by $\mathbf{3}^{\text{Br}}$ (0.003 mmol, 1.0 mol.%) and NaBPh_4 (0.015 mmol, 5.0 mol.%).

Determination of kinetic parameters and estimation of KIE

The activation enthalpy for DMAB dehydrogenation ($c_0 = 0.75$ M) was estimated experimentally from hydrogen evolution rates in 30–60°C temperature range. The initial rates (v_0) of DMAB conversion (Table S6) were obtained from the slopes of $\alpha(\text{DMAB})$ vs. time graphs derived from the hydrogen evolution data excluding the activation period. Then the corresponding activation enthalpy ($\Delta H^\ddagger = 14.5$ kcal/mol, Figure S26) was estimated from the initial rates of hydrogen evolution with Eyring's equation for bimolecular reaction in solution (Eq. 1).

$$v_0 \sim k_{\text{eff}} = \frac{k_{\text{B}}T}{h} e^{-\frac{\Delta H}{RT} + \frac{\Delta S}{T}} \quad (\text{Eq. 1})$$

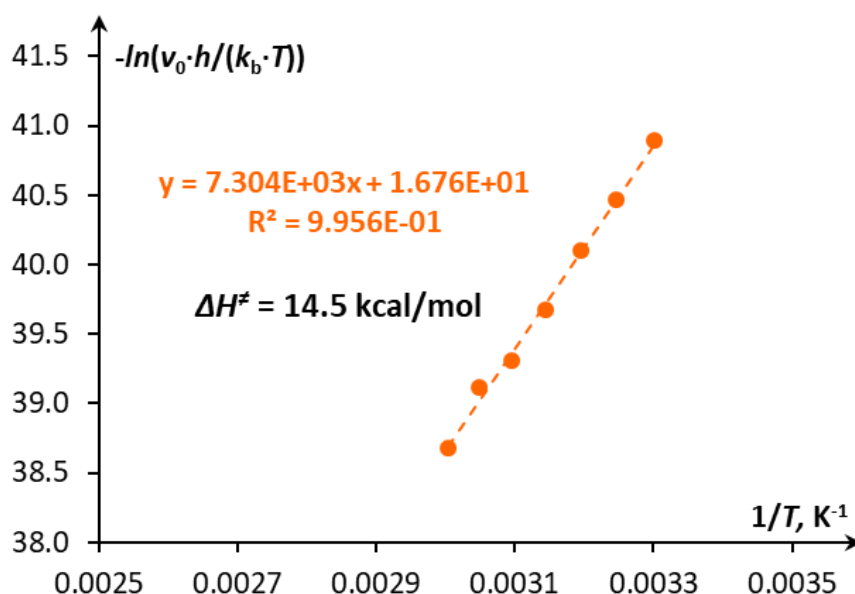


Figure S26. Eyring plot used for the determination of activation enthalpy for DMAB dehydrogenation in PhCl catalyzed by 3^{Br} /NaBPh₄ combination.

Table S6. Experimentally determined initial rates for DMAB dehydrogenation in PhCl in presence of 3^{Br} (0.1 mol%) and NaBPh₄ (1.0 mol%) at 30–60°C range obtained from pressure vs. time studies^a.

№	$T, ^\circ\text{C}$	T, K	Time, h	$v_0, \text{mol}\cdot\text{l}^{-1}\cdot\text{s}^{-1}$
1	30	303	17.7	$1.1\cdot 10^{-5}$
2	35	308	13.6	$1.7\cdot 10^{-5}$
3	40	313	10.6	$2.5\cdot 10^{-5}$
4	45	318	5.6	$3.9\cdot 10^{-5}$
5	50	323	3.9	$5.7\cdot 10^{-5}$
6	55	328	2.6	$7.0\cdot 10^{-5}$
7	60	333	2.1	$1.1\cdot 10^{-4}$

^a DMAB (1.5 mmol, 88.4 mg, $c_0 = 0.75$ M); 3^{Br} (0.0015 mmol, 0.9 mg); NaBPh₄ (0.015 mmol, 5.1 mg)

The linear shape of kinetic curves for hydrogen evolution (Figure S27) indicates pseudo-zero order in substrate, however measurements for dehydrogenation of various substrate loadings (0.75–2.25 mmol, $c_0 = 0.375$ – 1.125 M) by constant amount 3^{Br} (0.1 mol%, $c_0 = 0.75$ mM) and NaBPh₄ (1.0 mol%) revealed that an increase of substrate concentration leads to the corresponding linear increase of the reaction rate v_0 (Figure 27). This observation is consistent with the amine-borane participation in the catalyst activation (see below).

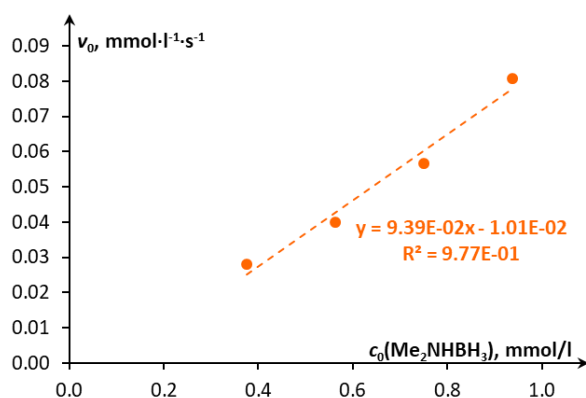


Figure S27. Plot of v_0 vs. c_0 for different concentrations of DMAB (0.75–2.25 mmol, $c_0 = 0.375$ –1.125 M) in PhCl at 50°C with constant catalyst loading of $\mathbf{3}^{\text{Br}}$ (0.1 mol%, 0.0015 mmol, $c_0 = 0.75$ mM) in presence of NaBPh₄ (5.1 mg, 1.0 mol%, 0.015 mmol).

Variation of the pre-catalyst loading gave linear dependence of the reaction rate on catalyst concentration meaning first order in catalyst (Figure S28). Kinetic isotope effects ($k_{\text{H}}/k_{\text{D}}$) were measured under same conditions at 60°C for deuterated substrates Me₂NHBD₃ (1.5±0.1), Me₂NDBH₃ (2.1±0.1) and Me₂NDBD₃ (2.9±0.1) (Table S7).

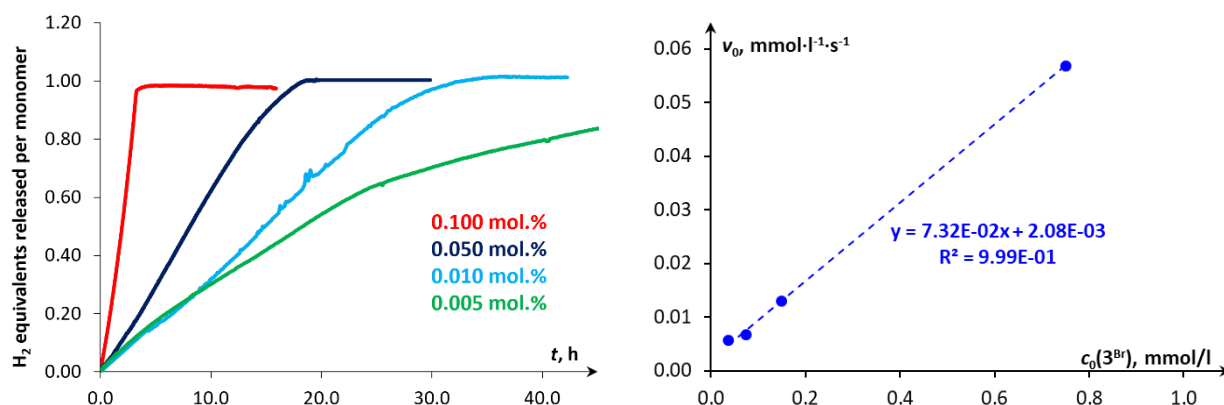


Figure S28. Hydrogen evolution kinetic curves (left) and v_0 vs. $c(\mathbf{3}^{\text{Br}})$ plot (right) for DMAB dehydrogenation at 50°C using various charge of $\mathbf{3}^{\text{Br}}$ (0.100, 0.050, 0.010 and 0.005 mol%) in the presence of NaBPh₄ (5.1 mg, 0.015 mmol).

Table S7. Experimentally determined initial rates for KIE estimation of DMAB (1.5 mmol, $c_0 = 0.75$ M) dehydrogenation catalyzed by $\mathbf{3}^{\text{Br}}$ (0.1 mol%) in the presence of NaBPh₄ (1.0 mol%) in PhCl at 60°C obtained from pressure vs. time studies.

No	DMAB	Time, h	v_0 , mol·l ⁻¹ ·s ⁻¹	KIE ($k_{\text{H}}/k_{\text{D}}$)
1	Me ₂ NHBH ₃	2.1	1.1·10 ⁻⁴	1.0
2	Me ₂ NDBH ₃	4.1	5.3·10 ⁻⁵	2.1
3	Me ₂ NHBD ₃	3.1	7.2·10 ⁻⁵	1.5
4	Me ₂ NDBD ₃	5.4	3.8·10 ⁻⁵	2.9

Modification of the loading of NaBPh₄ additive in a large range (0.125-to-8 mol%) show no significant effect for the reaction rate (Figure S29, Table S8) thus ruling out potential implication of Na⁺/Mn–H couple as a parallel catalytic cycle.

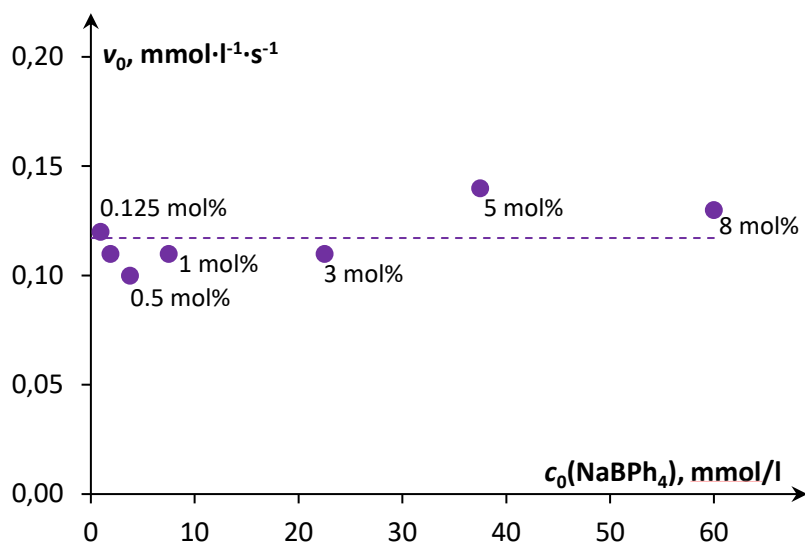


Figure S29. Plot of v_0 vs. c_0 for DMAB dehydrogenation in presence of different amounts of NaBPh₄ (0.25 – 8.0 mol%, $c_0 = 0.94$ – 60.0 mM) in PhCl at 60°C with constant catalyst loading of **3^{Br}** (0.1 mol%, 0.0015 mmol, $c_0 = 0.75$ mM).

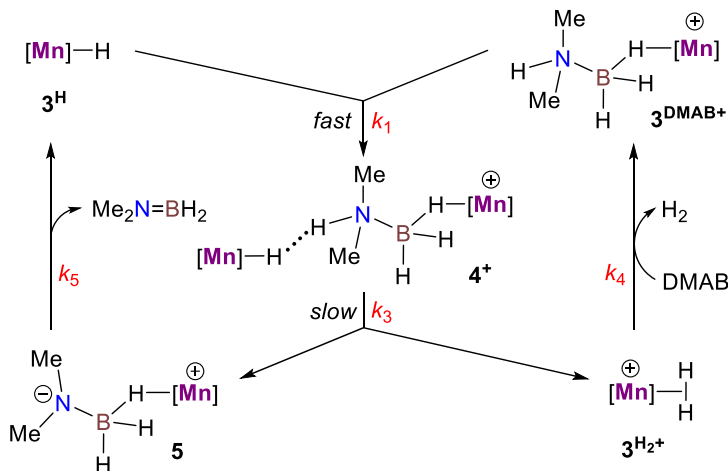
Table S8. Experimentally determined initial rates for DMAB dehydrogenation in PhCl in presence of **3^{Br}** (0.1 mol%) and NaBPh₄ (0.125-8.0 mol%) at 60°C obtained from pressure vs. time studies^a.

No	NaBPh ₄ loading, mol%	$c_0(\text{NaBPh}_4)$, mmol/L	Time, h	v_0 , mol·l ⁻¹ ·s ⁻¹
1	0.125	0.94	1.8	$1.2 \cdot 10^{-4}$
2	0.25	1.88	2.1	$1.1 \cdot 10^{-4}$
3	0.50	3.75	2.1	$1.0 \cdot 10^{-4}$
4	1.0	7.50	2.1	$1.1 \cdot 10^{-4}$
5	3.0	22.5	1.9	$1.1 \cdot 10^{-4}$
6	5.0	37.5	1.4	$1.4 \cdot 10^{-4}$
7	8.0	60.0	1.6	$1.3 \cdot 10^{-4}$

^a DMAB (1.5 mmol, 88.4 mg, $c_0 = 0.75$ M); **3^{Br}** (0.0015 mmol, 0.9 mg)

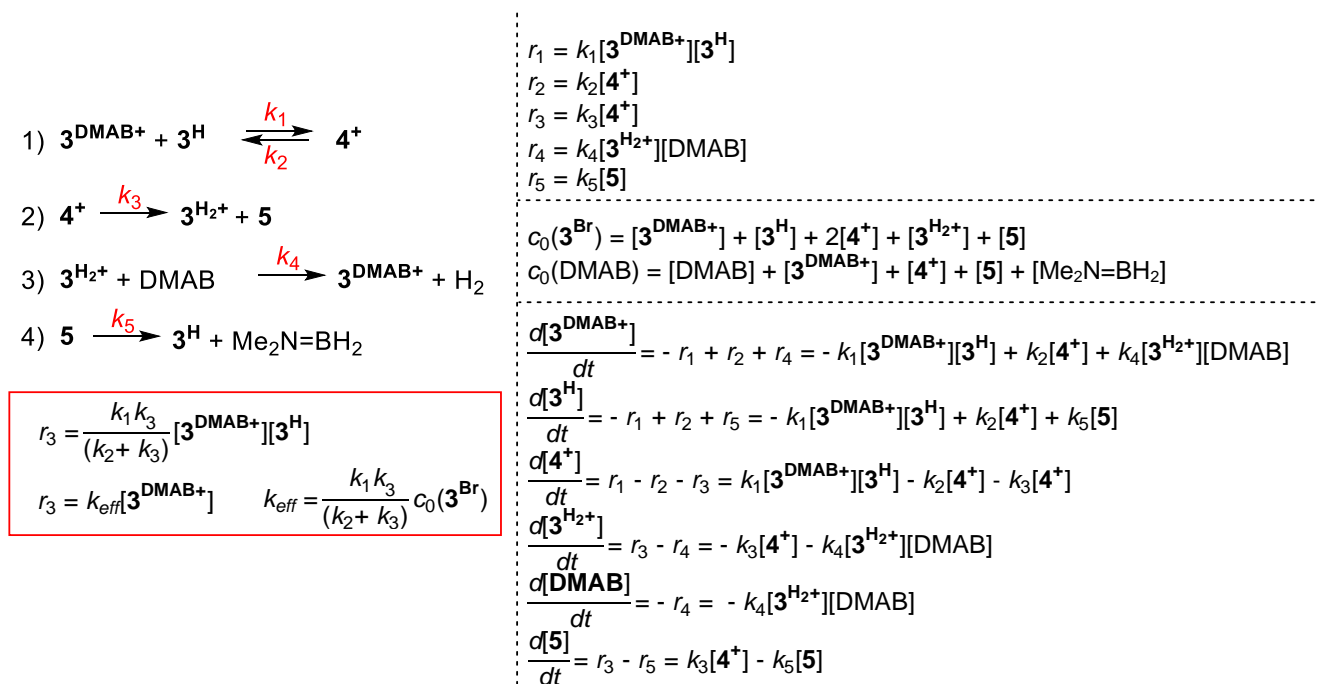
Analysis of kinetic data and mechanistic model

The active catalytic cycle starts from the interaction of 3^{DMAB^+} with 3^{H} to form 4^+ adduct (Scheme S1), which can either dissociate into initial reagents or undergo proton transfer from NH moiety to hydride complex 3^{H} . According to IR and NMR monitoring data, the cationic species quickly disappear at the beginning of the catalytic process and their concentration is too low to be detected during the active dehydrogenation stage. This allows us to propose that the proton transfer rate r_3 is higher than the rate of dissociation to initial metal complexes r_2 (Scheme S2, $k_3 \gg k_2$). Experimental KIE estimation (Table S7) and DFT calculations ($\Delta G^{\ddagger}_{\text{PT}} = 12.4$ kcal/mol and $\Delta G^{\ddagger}_{\text{HT}} = 3.4$ kcal/mol) indicated the proton transfer to be the rate-determining step followed by almost barrierless hydride transfer ($k_3 \ll k_5$). The detection of hydride 3^{H} in virtually constant concentration during spectroscopic monitoring suggests the hydride transfer to be faster than hydrogen evolution from $3^{\text{H}2^+}$ ($k_5 \gg k_4$). The equilibrium shift due to fast hydride transfer and evolution of hydrogen leads to irreversibility of steps 2–4 (Scheme S2). Thus, the reaction



Scheme S1. Simplified catalytic cycle for DMAB dehydrogenation catalyzed by complex 3^{Br}

scheme can be simplified to the following kinetic equations, where the overall process rate is limited by a proton transfer and equal to $r_3 = k_3[4^+]$. Applying quasi-stationary state approximation for the formation rates of 3^{DMAB^+} and 3^{H} ($d[3^{\text{DMAB}^+}]/dt = 0$, $d[3^{\text{H}}]/dt = 0$), the concentration of 4^+ can be expressed as $[4^+] = (k_1/(k_2+k_3))[3^{\text{DMAB}^+}][3^{\text{H}}]$. During the active catalytic dehydrogenation, 3^{H} was observed in IR spectra as a major Mn(I) species $[3^{\text{H}}] \gg [3^{\text{DMAB}^+}]$ with a constant concentration $[3^{\text{H}}] \approx c_0(3^{\text{Br}})$. In this case an excess of $[3^{\text{H}}]$ in the reaction mixture leads to the pseudo-first order reaction kinetics and the reaction rate can be approximated with $r = k_{\text{eff}}[3^{\text{DMAB}^+}]$, where $k_{\text{eff}} = (k_1 k_3 / (k_2 + k_3)) c_0(3^{\text{Br}})$.



Scheme S2. Rate law equations for DMAB dehydrogenation catalyzed by complex 3^{Br} .

DFT calculations.

Calculations were performed with the Gaussian 09¹⁰ package at the DFT/ ω B97XD level¹¹ without any ligand simplification. For all atoms, the Def2-TZVP basis¹² set was applied. The structures of all complexes were fully optimized in toluene ($\epsilon=2.3741$) described by the SMD model,¹³ without any symmetry restrictions. The nature of all the stationary points on the potential energy surfaces was confirmed by vibrational analysis. Relaxed potential energy surfaces scans are done under same approach with the Def2-SVP basis set.

DFT calculations showed that manganese bis(NHC) hydride complex 3^H has three minima on its potential energy surface corresponding to three isomers *fac,syn-3^H*, *fac,anti-3^H* and *mer-3^H* (Figure S30) similarly as it was previously found for its dppe analogue (dppe) $Mn(CO)_3H$.^{3,14} The optimized geometry of *fac,syn-3^H* reproduced well the corresponding X-ray crystal structure.⁶ Two facial isomers *fac,syn-3^H* and *fac,anti-3^H* differ by the position of CH_2 bridge related to the hydride ligand in the chelating six-membered cycle. While *fac,syn-3^H* is slightly more stable than *fac,anti-3^H* (Table S9), *mer-3^H* was found to be strongly disfavored ($\Delta H^{298} +3.2$ kcal, $\Delta G^{298} +3.0$ kcal/mol). Facial isomers *fac,syn-3^H* and *fac,anti-3^H* can easily interconvert under reaction conditions by the flip of six-membered cycle ($\Delta G^{\#298} = 11.0$ kcal/mol). In contrast, the transformation of *fac,syn-3^H* into *mer-3^H* by the rotation of the $[Mn(CO)_3H]$ moiety¹⁴ is much more energy demanding ($\Delta G^{\#298} = 26.9$ kcal/mol). Taking into account much lower thermodynamic stability of meridional Mn(I) species and elevated *fac-to-mer* isomerization barriers, we considered only *facial* complexes for the reaction mechanism calculations.

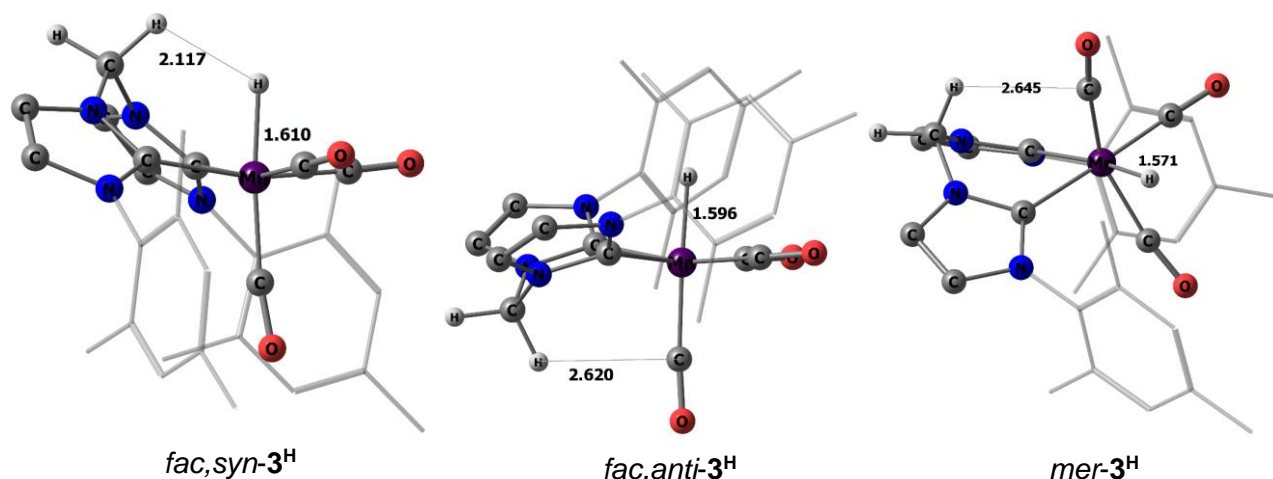


Figure S30. Optimized geometry of three isomers of hydride complex 3^H (Mes groups are shown as wireframe and most of hydrogen atoms are omitted for clarity).

Table S9. Calculated thermodynamic parameters for two facial isomers of Mn(I) complexes 3^H , $3^H \cdots DMAB$, 3^+ , 3^{DMAB+} and 3^{H_2+} (kcal/mol at 298K, data referred to *fac,syn-* species)

Complex	3^H	$3^H \cdots DMAB$	3^+	3^{DMAB+}	3^{H_2+}
	$\Delta E, \Delta H, \Delta G$				
<i>fac,syn-</i>	0.0, 0.0, 0.0	0.0, 0.0, 0.0	0.0, 0.0, 0.0	0.0, 0.0, 0.0	0.0, 0.0, 0.0
<i>fac,anti-</i>	2.1, 1.6, 0.3	0.2, 0.0, 0.1	-2.5, -2.1, -1.9	3.2, 3.4, 5.0	-1.5, -1.3, -1.7

The interaction of 3^H with DMAB leads to the formation of two almost isoergic facial isomers of $3^H \cdots DMAB$ adduct (Figure S31). While metrical parameters in *fac,syn-3^H...DMAB* correspond well to typical dihydrogen bonding adduct, *fac,anti-3^H...DMAB* is mostly stabilized by van der Waals interactions. All attempts to perform a proton transfer from *fac,syn-3^H...DMAB* under experimentally relevant conditions failed since activation barriers higher than 30 kcal/mol were observed without any stabilization of the resulting products (Figure S31, right).

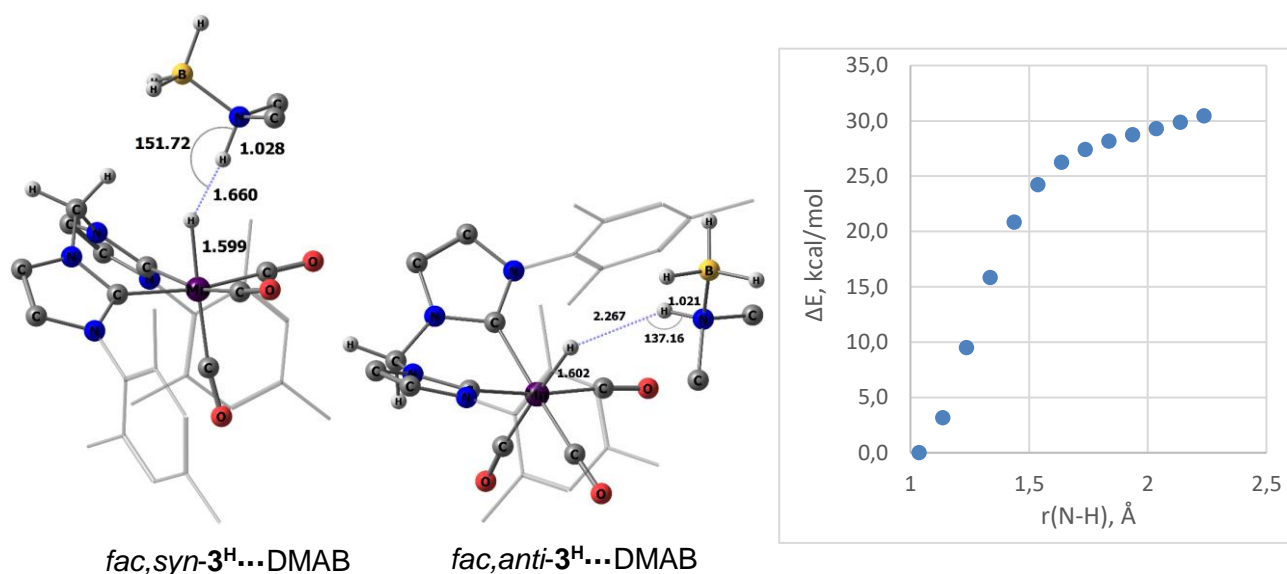


Figure S31. Optimized geometry of two facial isomers of $3^{\text{H}}\dots\text{DMAB}$ adduct (Mes groups are shown as wireframe and most of hydrogen atoms are omitted for clarity) and potential energy profile upon increasing N–H bond in *fac,syn-3^H...DMAB* (right).

In case of cationic 16-e complexes 3^+ (Figure S32), *fac,anti*-isomer was slightly more stable (Table S9) probably due to the occurrence of agostic C–H interaction with one of the proximal methyl groups, similarly as it was previously shown in related cationic Mn(I) diphosphine¹⁵ and NHC¹⁶ derivatives.

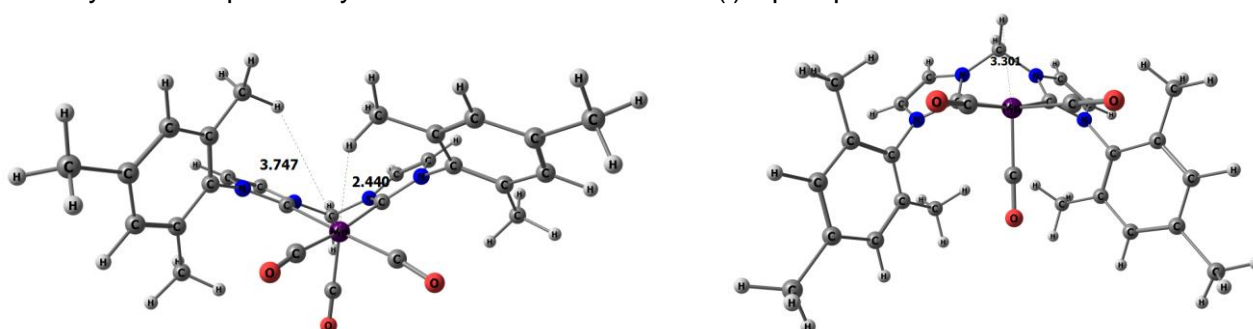


Figure S32. Optimized geometry of facial isomers of cationic complex 3^+ .

In contrast, for complex 3^{DMAB^+} *fac,syn*-isomer was much more stable (Table S9) and no reliable pathway for hydride transfer from the coordinated DMAB to the metal was located (Figure S33, right).

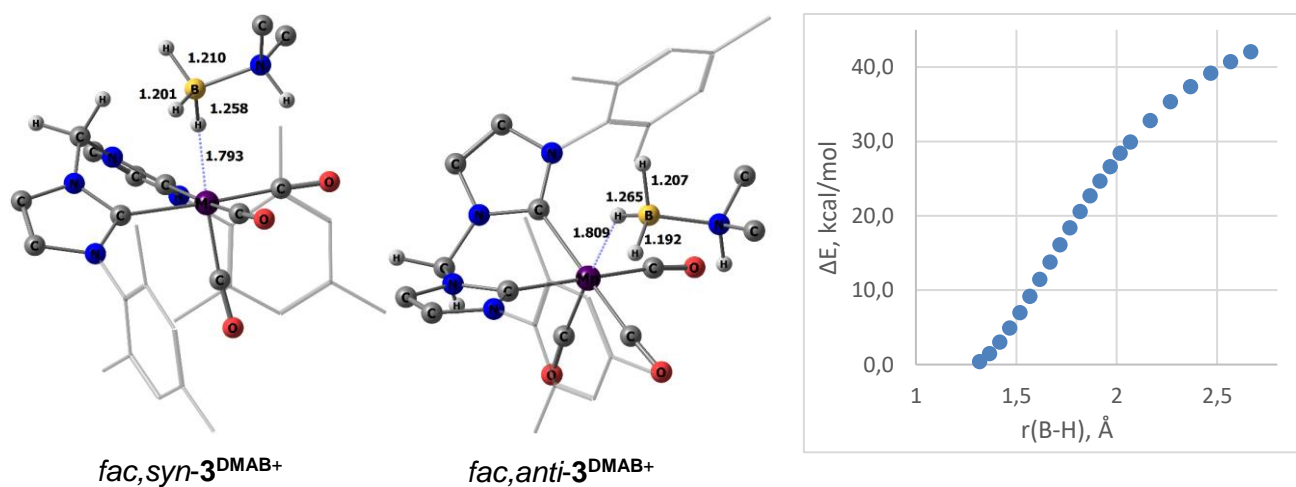


Figure S33. Optimized geometry of two facial isomers of 3^{DMAB^+} (Mes groups are shown as wireframe and most of hydrogen atoms are omitted for clarity) and potential energy profile upon increasing B–H bond in *fac,syn-3^{DMAB+}* (right).

Calculated energy profiles for DMAB dehydrogenation catalyzed by $3^+/3^H$ couple having *fac,syn*-conformation of metal fragments are presented in Figure S34. Optimized geometry of binuclear and mononuclear reaction intermediates are shown in Figure S35 and Figure S36, respectively.

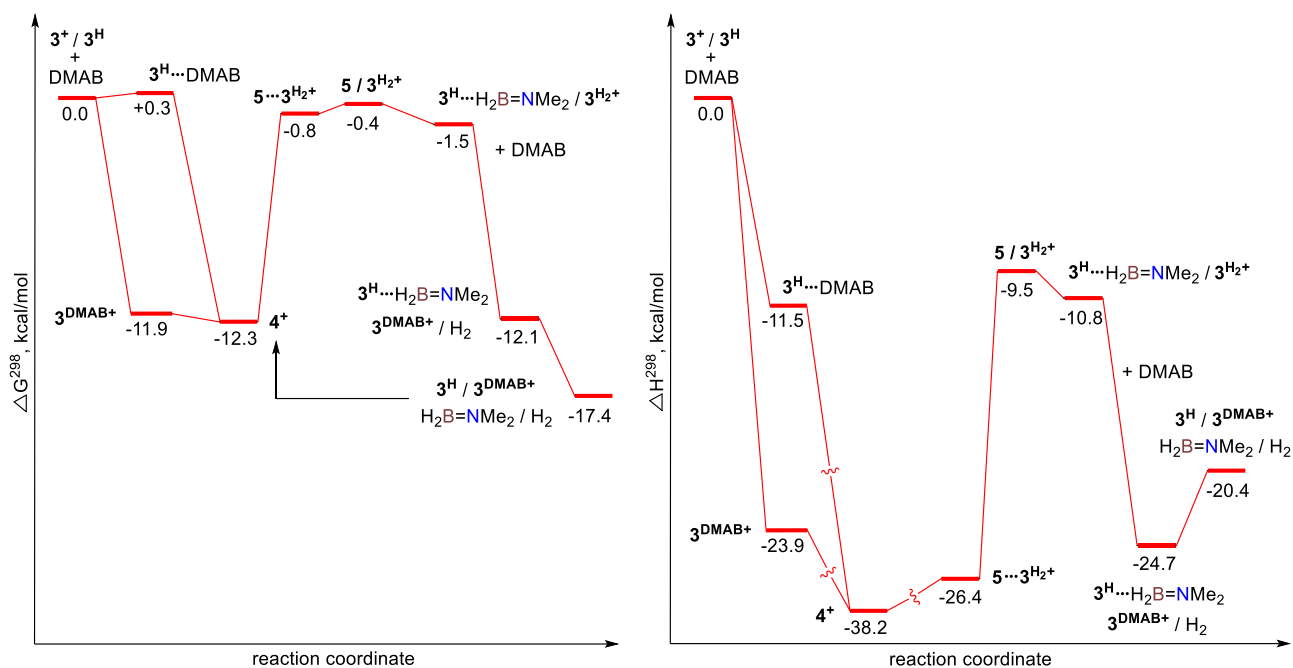


Figure S34. ΔG^{298} and ΔH^{298} energy profiles for DMAB dehydrogenation catalyzed by $3^+/3^H$ couple (both metallic fragments are in *fac,syn*-conformation).

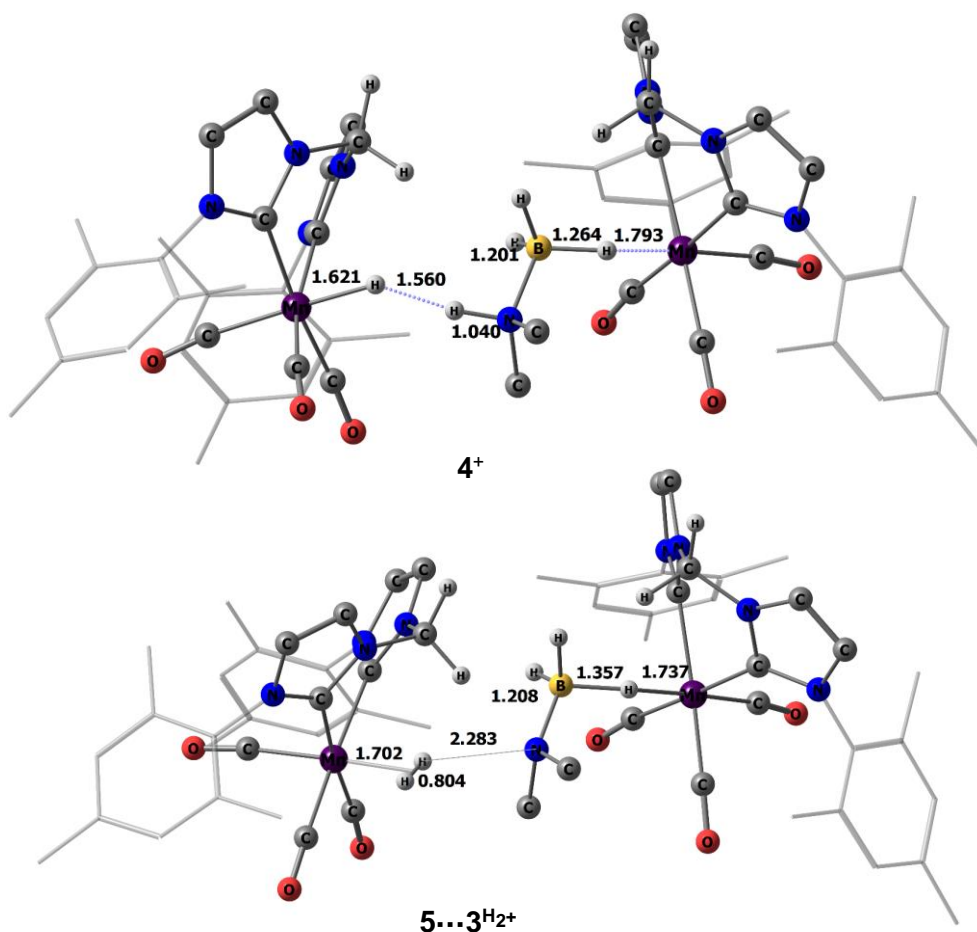


Figure S35. Optimized geometry of complexes 4^+ and $5 \cdots 3^H_2^+$ (Mes groups are shown as wireframe and most of hydrogen atoms are omitted for clarity).

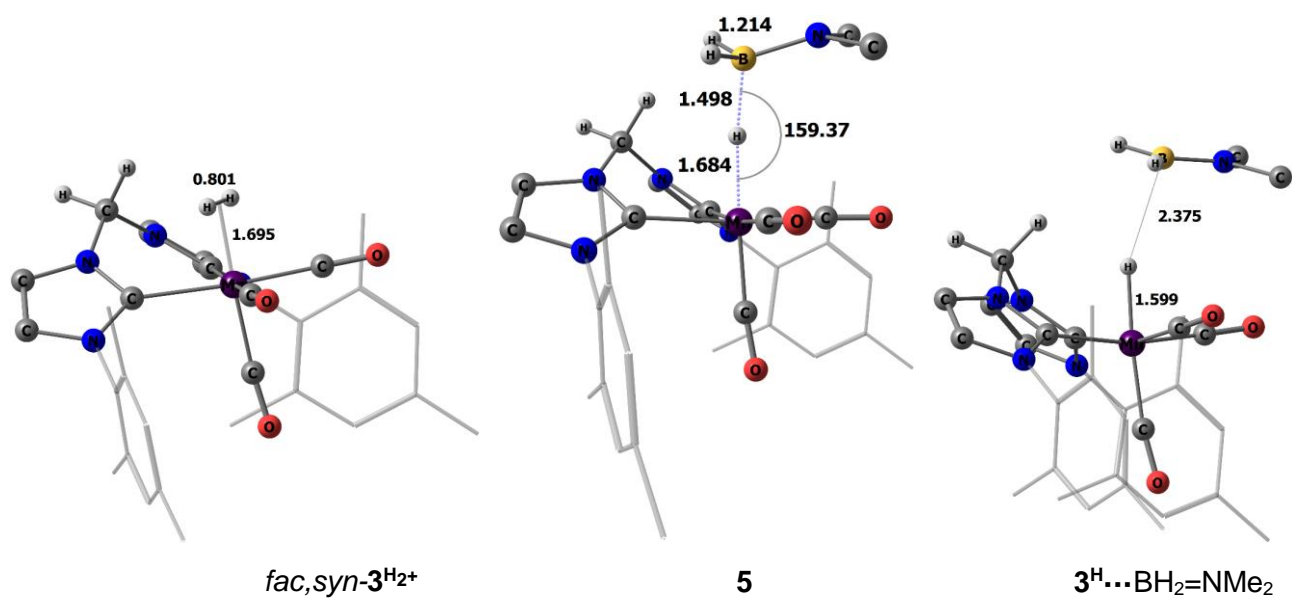


Figure S36. Optimized geometry of $3^{\text{H}_2^+}$, **5** and $3^{\text{H}}\dots\text{BH}_2=\text{NMe}_2$ (Mes groups are shown as wireframe and most of hydrogen atoms are omitted for clarity).

References.

- 1 L. Wirtz, W. Haider, V. Huch, M. Zimmer and A. Schäfer, *Chem. Eur. J.*, 2020, **26**, 6176–6184.
- 2 Y. Yang, Z. Zhang, X. Chang, Y.-Q. Zhang, R.-Z. Liao and L. Duan, *Inorg. Chem.*, 2020, **59**, 10234–10242.
- 3 E. S. Osipova, E. S. Gulyaeva, N. V. Kireev, S. A. Kovalenko, C. Bijani, Y. Canac, D. A. Valyaev, O. A. Filippov, N. V. Belkova and E. S. Shubina, *Chem. Commun.*, 2022, **58**, 5017–5020.
- 4 E. S. Osipova, S. A. Kovalenko, E. S. Gulyaeva, N. V. Kireev, A. A. Pavlov, O. A. Filippov, A. A. Danshina, D. A. Valyaev, Y. Canac, E. S. Shubina and N. V. Belkova, *Molecules*, 2023, **28**, 3368.
- 5 R. Buhaibeh, O. A. Filippov, A. Bruneau-Voisine, J. Willot, C. Duhayon, D. A. Valyaev, N. Lugan, Y. Canac and J.-B. Sortais, *Angew. Chem. Int. Ed.*, 2019, **58**, 6727–6731.
- 6 K. Azouzi, L. Pedussaut, R. Pointis, A. Bonfiglio, R. Kumari Riddhi, C. Duhayon, S. Bastin and J.-B. Sortais, *Organometallics*, 2023, **42**, 1832–1838.
- 7 L. J. Farrugia, *J. Appl. Crystallogr.*, 2012, **45**, 849–854.
- 8 M. C. Burla, R. Caliandro, B. Carrozzini, G. L. Casciarano, C. Cuocci, C. Giacovazzo, M. Mallamo, A. Mazzone and G. Polidori, *J. Appl. Cryst.*, 2015, **48**, 306–309.
- 9 G. M. Sheldrick, *Acta Crystallogr., Sect. A: Found. Crystallogr.*, 2008, **64**, 112.
- 10 M. J. Frisch, G. W. Trucks, H. B. Schlegel, G. E. Scuseria, M. A. Rob, J. R. Cheeseman, J. A. M. Jr., T. Vreven, K. N. Kudin, J. C. Burant, J. M. Millam, S. S. Iyengar, J. Tomasi, V. Barone, B. Mennucci, M. Cossi, G. Scalmani, N. Rega, G. A. Petersson, H. Nakatsuji, M. Hada, M. Ehara, K. Toyota, R. Fukuda, J. Hasegawa, M. Ishida, T. Nakajima, Y. Honda, O. Kitao, H. Nakai, M. Klene, X. Li, J. E. Knox, H. P. Hratchian, J. B. Cross, V. Bakken, C. Adamo, J. Jaramillo, R. Gomperts, R. E. Stratmann, O. Yazyev, A. J. Austin, R. Cammi, C. Pomelli, J. W. Ochterski, P. Y. Ayala, K. Morokuma, G. A. Voth, P. Salvador, J. J. Dannenberg, V. G. Zakrzewski, S. Dapprich, A. D. Daniels, M. C. Strain, O. Farkas, D. K. Malick, A. D. Rabuck, K. Raghavachari, J. B. Foresman, J. V. Ortiz, Q. Cui, A. G. Baboul, S. Clifford, J. Cioslowski, B. B. Stefanov, G. Liu, A. Liashenko, P. Piskorz, I. Komaromi, R. L. Martin, D. J. Fox, T. Keith, M. A. Al-Laham, C. Y. Peng, A. Nanayakkara, M. Challacombe, P. M. W. Gill, B. Johnson, W. Chen, M. W. Wong, C. Gonzalez and J. A. Pople, *Gaussian, Inc.*, Wallingford, CT, 2009.
- 11 J.-D. Chai and M. Head-Gordon, *Phys. Chem. Chem. Phys.*, 2008, **10**, 6615–6620.
- 12 (a) F. Weigend and R. Ahlrichs, *Phys. Chem. Chem. Phys.*, 2005, **7**, 3297–3305; (b) F. Weigend, *Phys. Chem. Chem. Phys.*, 2006, **8**, 1057–1065.
- 13 A. V. Marenich, C. J. Cramer and D. G. Truhlar, *J. Phys. Chem. B*, 2009, **113**, 6378–6396.
- 14 N. V. Kireev, O. A. Filippov, E. S. Gulyaeva, E. S. Shubina, L. Vendier, Y. Canac, J.-B. Sortais, N. Lugan and D. A. Valyaev, *Chem. Commun.*, 2020, **56**, 2139–2142.
- 15 (a) W. A. King, X.-L. Luo, B. L. Scott, G. J. Kubas and K. W. Zilm, *J. Am. Chem. Soc.*, 1996, **118**, 6782–6783; (b) A. Toupadakis, G. J. Kubas, W. A. King, B. L. Scott and J. Huhmann-Vincent, *Organometallics*, 1998, **17**, 5315–5323; (c) W. A. King, B. L. Scott, J. Eckert and G. J. Kubas, *Inorg. Chem.*, 1999, **38**, 1069–1084.
- 16 T. A. Martin, C. E. Ellul, M. F. Mahon, M. E. Warren, D. Allan and M. K. Whittlesey, *Organometallics*, 2011, **30**, 2200–2211.